Research Square

Preprints are preliminary reports that have not undergone peer review.
They should not be considered conclusive, used to inform clinical practice,
or referenced by the media as validated information.

Beyond accelerated aging: Multi-organ aging imbalance predicts adverse health outcomes

Yucan Li
Fudan University https://orcid.org/0000-0002-9778-9057
Xinming Xu
Fudan University
Xinyi He
Fudan University
Yi Zheng
Fudan University
Chen Suo
Fudan University
Zhenqiu Liu
Fudan University
Ziyu Yuan
Fudan University Taizhou Institute of Health Sciences
Yanfeng Jiang
Fudan University
Kelin Xu
xukelin@fudan.edu.cn

Fudan University School of Public Health https://orcid.org/0000-0002-6788-4256
Xingdong Chen
xingdongchen@fudan.edu.cn

Fudan University

Research Article

Keywords: Multi-organ aging imbalance, Organ-specific aging, Biological age, Mortality, Multimorbidity, Frailty

Posted Date: November 9th, 2026

DOI: https://doi.org/10.21203/rs.3.rs-11629199/v1

License: This work is licensed under a Creative Commons Attribution 4.0 International License.
Read Full License

Additional Declarations: The authors declare no competing interests.

Beyond accelerated aging: Multi-organ aging imbalance predicts adverse health outcomes

Yucan Li[1,2], Xinming Xu[3], Xinyi He[1], Yi Zheng[1], Chen Suo[4,5], Zhenqiu Liu[1], Ziyu Yuan[5], Yanfeng Jiang[1], Kelin Xu[2,4*], Xingdong Chen[1,5*]

[1] State Key Laboratory of Genetics and Development of Complex Phenotypes, School of Public Health, National Clinical Research Center for Aging and Medicine, Huashan Hospital, Fudan University, Shanghai 200032, China.

[2] Department of Biostatistics, School of Public Health, The Key Laboratory of Public Health Safety of Ministry of Education, Fudan University, Shanghai 200032, China.

[3] Department of Nutrition and Food Hygiene, Ministry of Education Key Laboratory of Public Health Safety, School of Public Health, Institute of Nutrition, Fudan University, Shanghai 200032, China.

[4] School of Public Health, and the Key Laboratory of Public Health Safety of Ministry of Education, Fudan University, Shanghai, 200032, China.

[5] Fudan University Taizhou Institute of Health Sciences, Taizhou, Jiangsu 225326, China.

***Corresponding authors**

Kelin Xu

Department of Biostatistics, School of Public Health, The Key Laboratory of Public Health Safety of Ministry of Education, Fudan University, Shanghai 200032, China.

Email: xukelin@fudan.edu.cn

Xingdong Chen

State Key Laboratory of Genetics and Development of Complex Phenotypes, School of Public Health, National Clinical Research Center for Aging and Medicine, Huashan Hospital, Fudan University, Shanghai 200032, China.

Email: xingdongchen@fudan.edu.cn

Abstract

Biological aging varies across organ systems, yet the extent of this cross-organ dispersion and its implications for health remain poorly characterized. We quantified this dispersion as multi-organ aging imbalance, using the within-person standard deviation of standardized biological-age deviations across six organ systems in 221,599 UK Biobank participants. Higher multi-organ aging imbalance was independently associated with all-cause mortality (HR per 1-s.d. increase, 1.11; 95% CI, 1.09–1.13), six incident organ-disease outcomes and three multimorbidity transitions after adjustment for overall biological-age deviation, chronological age and sex. Notably, greater imbalance was associated with elevated mortality risk even among individuals with relatively low overall biological aging (HR, 1.09; 95% CI, 1.03–1.16). Associations with mortality were validated in five external cohorts. In separate analyses restricted to ELSA and CHARLS, higher imbalance was associated with greater frailty burden and incident frailty. Enrichment analysis of proteins associated with imbalance highlighted amino acid and fatty acid metabolism, immune signaling, telomere organization and DNA repair. Associations were robust across alternative imbalance definitions and persisted after excluding organs with extreme age deviations, with similar findings observed using 11 protein-derived organ ages. Together, these findings highlight cross-organ aging dispersion as a complementary dimension of biological aging with implications for health vulnerability.

Key words: Multi-organ aging imbalance; Organ-specific aging; Biological age; Mortality; Multimorbidity; Frailty

Introduction

Biological aging is a heterogeneous process that varies substantially among individuals of the same chronological age[1,2]. To capture this variation, biological age measures have been developed using clinical biomarkers, physiological characteristics, and molecular profiles, providing insights into age-related functional decline and disease susceptibility[3,4]. Growing evidence further suggests that biological aging varies across organs and physiological systems within individuals[1,5]. Advances in organ-specific biological age estimation, using clinical phenotypes, imaging, and plasma proteomics, have enabled the characterization of aging across multiple organ systems[1,5]. These studies have linked organ-specific aging to corresponding diseases, multimorbidity, and mortality, while revealing interrelationships among aging processes across organ systems[1,5,6].

Despite these advances, existing research has largely focused on the magnitude of aging in individual organs, the number of accelerated-aging organs, or specific patterns of multi-organ aging[5,7,8]. Although these approaches have provided valuable insights, less attention has been paid to the degree of divergence in biological aging across organs within the same individual. The distribution of organ-specific biological-age deviations may vary considerably across individuals, with some exhibiting relatively uniform aging across organs and others showing pronounced differences, with certain organs appearing biologically older and others younger. Such variation raises the possibility that cross-organ dispersion represents an additional characteristic of individual aging profiles, complementing existing descriptions of organ-specific aging. However, the extent of this within-individual dispersion remains insufficiently quantified, and its implications for health are poorly understood.

Here, we systematically investigated multi-organ aging imbalance in 221,599 UK Biobank (UKB) participants. We developed biological-age models for six organ systems using routine clinical biomarkers and quantified imbalance as the within-person dispersion of standardized organ-specific biological-age deviations (**Fig. 1**). We examined its associations with all-cause mortality, incident organ diseases and multimorbidity transitions, while accounting for overall biological-age deviation. We also investigated the

joint associations of imbalance and overall biological-age deviation with mortality, evaluated the reproducibility of mortality associations across five external cohorts and examined associations with frailty. In addition, we explored lifestyle, psychosocial, socioeconomic and proteomic correlates of imbalance, and extended the framework to organ ages estimated using published proteomic models[7].

Results

Routine clinical biomarkers yield phenotype-derived biological ages across organ systems

We developed phenotype-derived biological ages across six organ systems in UKB, with five external cohorts contributing replication and extension analyses (**Supplementary Table 1**). Models were developed in 155,119 UKB participants and evaluated in an independent test set of 66,480 participants (**Methods**). Routine clinical biomarkers were organized into cardiovascular, pulmonary, immune, renal, hepatic and metabolic systems. We constructed biological ages by mapping biomarker-associated risk of the corresponding organ disease onto an age scale. The overall biological age was derived using biomarkers from all six systems, with all-cause mortality as the modelling outcome (**Methods**). The final sex-specific equations expressed biological age as a weighted linear combination of chronological age and the retained biomarkers (**Fig. 2a**; **Supplementary Table 2**). Age-adjusted deviations from these measures were termed organ AgeDev and overall AgeDev, respectively. For each biological-age measure, agreement with chronological age was comparable between the training and test sets (**Supplementary Fig. 1**). Age- and sex-adjusted partial correlations among the six organ AgeDev measures were positive but mostly modest, ranging from r=0.03 for the pulmonary–renal pair to r=0.39 for the cardiovascular–metabolic pair (**Fig. 2b**). The corresponding correlations with overall AgeDev ranged from r=0.22 for renal AgeDev to r=0.66 for immune AgeDev (**Fig. 2b**).

In the UKB test set, higher overall AgeDev was associated with all six disease groups after adjustment for age and sex (HRs per 1-s.d. increase, 1.37–2.23; **Extended Data Fig. 1a**). In mutually adjusted models including all six organ-specific AgeDev measures, overall AgeDev, age and sex, the AgeDev measure

corresponding to each disease outcome had the largest HR point estimate among the six organ-specific measures in five of the six incident disease groups (**Fig. 2c**; **Supplementary Table 3**). These associations were generally similar after further adjustment for ethnicity, smoking, alcohol consumption and education (**Extended Data Fig. 1b**), and between the training and test sets (**Extended Data Fig. 1c**). Conventional machine-learning biological-age models (elastic net regression, linear support vector regression and XGBoost) showed positive associations with the corresponding disease outcomes, with generally smaller HR point estimates than the primary models (**Extended Data Fig. 1d**; **Supplementary Table 4**). Organ AgeDev measures derived from published proteomic aging models likewise showed generally smaller HR point estimates than the corresponding phenotype-derived measures (**Fig. 2d**). Across cohorts, meta-analyses combining UKB test-set estimates with available estimates from the China Health and Retirement Longitudinal Study (CHARLS), the English Longitudinal Study of Ageing (ELSA), the Shanghai Suburban Adult Cohort and Biobank (SSACB) and the Taizhou Longitudinal Study (TZL) yielded pooled HRs of 1.19-2.11 for corresponding organ-disease associations (**Fig. 2e**; **Supplementary Table 3**). In the US National Health and Nutrition Examination Survey (NHANES), higher AgeDev in each of the six organ systems was associated with all-cause mortality (**Supplementary Fig. 2**). In identical outcome-specific UKB test-set risk sets, all nine cohort-compatible refits retained positive disease associations, with HR point estimates generally modestly lower than those of the corresponding primary models (**Supplementary Table 5**).

Multi-organ aging imbalance is associated with adverse health outcomes beyond overall biological aging

We next quantified the dispersion of organ aging within the same individual. For each participant, multi-organ imbalance was calculated as the within-person standard deviation of the six UKB organ AgeDev z-scores and was subsequently standardized across participants for analysis. Mean organ AgeDev was defined as the within-person average of these organ AgeDev *z*-scores in each cohort. Across 221,599 UKB participants, imbalance was moderately correlated with mean organ AgeDev (r=0.311, $P < 0.001$) and overall AgeDev (r=0.302, $P < 0.001$; **Fig. 3a**). In UKB, median imbalance was higher in older

chronological-age groups (Kruskal-Wallis $P=1.23 \times 10^{-219}$; **Fig. 3b**). Age-group differences were also observed externally (**Extended Data Fig. 2**), whereas sex differences varied in direction and statistical significance across cohorts (**Supplementary Fig. 3**). Repeated-measure analyses showed positive within-person changes in imbalance across follow-up waves in both CHARLS and ELSA (**Fig. 3c**).

In UKB, greater imbalance was associated with all-cause mortality (HR per 1-s.d. increase, 1.11; 95% CI, 1.09-1.13), all six incident organ-disease endpoints (HR range, 1.06–1.17) and all three multimorbidity transitions (HR range, 1.07–1.14) in models adjusted for overall AgeDev, age and sex (**Fig. 3d**; **Supplementary Table 6**). Further demographic/technical, socioeconomic and lifestyle adjustment produced similar estimates. Adding the corresponding organ AgeDev or replacing overall AgeDev with mean organ AgeDev attenuated some organ-disease associations, but most remained statistically significant (**Fig. 3d**; **Supplementary Fig. 4a**). Alternative dispersion metrics, organ standardization and restriction to the middle 80% of the imbalance distribution generally supported the main pattern (**Extended Data Fig. 3a,b**). To assess whether the associations depended on a single extreme organ, we excluded each participant's most-extreme organ and recalculated mean organ AgeDev and imbalance from the remaining five organs; HRs remained above one across all ten outcomes (**Extended Data Fig. 3c**). Results were also broadly consistent after excluding the outcome-matched organ or both the highest and lowest organs (**Extended Data Fig. 3c**). HR estimates varied less between subsets as more organs were included across all three-, four- and five-organ subsets (**Extended Data Fig. 3d**). We also assessed incremental model fit and apparent discrimination after adding imbalance. Adding imbalance to models containing traditional risk factors and overall AgeDev improved model fit across the main UKB outcomes in likelihood-ratio tests, although apparent C-index gains (0.0004–0.0035) were modest (**Supplementary Table 7**).

Across the five external cohorts, higher imbalance was associated with all-cause mortality (HR range per 1-s.d. increase, 1.08-1.27; adjusted for mean organ AgeDev, age and sex; **Fig. 3e**). Available organ-disease analyses showed endpoint-specific support after the same adjustment, including pulmonary disease in ELSA, kidney disease in SSACB, and metabolic and liver disease in TZL (**Supplementary Fig. 4b,c**). Frailty analyses extended this evidence to functional aging outcomes. Higher imbalance was associated with

greater frailty burden and higher incident frailty risk in ELSA and CHARLS (ELSA HR 1.06, 95% CI 1.01-1.12; CHARLS HR 1.06, 95% CI 1.01–1.10; **Fig. 3f,g**; **Supplementary Table 8**).

Multi-organ imbalance stratifies risk within levels of overall aging

To characterize organ-aging patterns at the extremes of the imbalance distribution, we first used the 10th and 90th percentiles of imbalance to define the bottom decile, middle 80% and top decile. Within each tail, the six standardized organ AgeDev values were used as clustering features. Clustering identified six top-decile profiles (T1–T6), with marked deviations in individual organs or contrasting deviations across organs; the bottom decile was represented by two descriptive profiles with broadly lower (B1) or higher (B2) AgeDev across all six organs (**Fig. 4a**). After adjustment for age, sex and overall AgeDev, all six top-decile profiles were associated with higher all-cause mortality than the middle 80% (HR range 1.17–1.33; **Fig. 4a**). T5 combined lower mean organ AgeDev (mean −0.82 s.d.) with marked imbalance and an overall AgeDev close to the population average (mean 0.06 s.d.), yet was associated with higher mortality than the middle 80% (HR 1.17, 95% CI 1.03–1.33; **Fig. 4a**).

We then examined joint strata of imbalance and overall AgeDev across the full UKB analysis population. Median splits of overall AgeDev and imbalance defined Low/Low, Low/High, High/Low and High/High groups in UKB (**Fig. 4b**). The Low/High group had modestly higher all-cause mortality risk than Low/Low despite sharing the lower overall-AgeDev stratum (HR 1.09, 95% CI 1.03–1.16). Within the higher overall-AgeDev stratum, High/High had a higher mortality HR point estimate than High/Low (2.50 versus 1.72 relative to Low/Low; **Fig. 4b**). This pattern extended beyond mortality: Low/High generally had higher organ-disease and multimorbidity risk than Low/Low, whereas High/High generally had higher point estimates than High/Low across organ-disease and multimorbidity outcomes (**Extended Data Fig. 4**). In external frailty analyses based on mean organ AgeDev, Low/High likewise had higher risk than Low/Low (ELSA HR 1.30, 95% CI 1.13–1.49; CHARLS HR 1.13, 95% CI 1.01–1.27). High/High likewise showed higher point estimates than High/Low, with partially overlapping confidence intervals (ELSA HR 2.00, 95% CI 1.75-2.27; CHARLS HR 1.31, 95% CI 1.17–1.47; **Fig. 4c**; **Supplementary Table 9**).

Exposure and proteomic correlates of multi-organ imbalance

We next examined lifestyle, psychosocial and socioeconomic correlates of multi-organ imbalance in UKB. Among 21 indicators coded in favourable directions, all age- and sex-adjusted beta estimates were negative and 20 reached a false discovery rate (FDR) < 0.05 (**Fig. 5a**). After additional adjustment for overall AgeDev, 17 indicators remained inversely associated with imbalance at FDR<0.05 (**Fig. 5a**; **Supplementary Table 10**).

As for molecular correlates, among 19,744 participants with both phenotype and proteomic measurements, phenotype-derived imbalance was positively associated with 742 proteins and negatively associated with 126 of the 2,916 proteins tested. These associations met FDR<0.05 after adjustment for overall AgeDev, age, sex and body mass index (**Fig. 5b**; **Supplementary Data 1**). Gene set enrichment analysis (GSEA) of the protein-ranked results identified 117 significant pathways, which were organized into 48 modules. Pathways with positive normalized enrichment scores (NES) included amino acid and fatty acid metabolism, biological oxidation, and immune-effector and cytokine signaling, whereas those with negative NES included telomere organization, DNA repair, and cell-cycle or mitotic programs (**Fig. 5c**; **Supplementary Table 11** and **Supplementary Data 2**).

Multi-organ imbalance extends to protein-derived organ aging

We then applied the imbalance framework to organ ages estimated using published proteomic aging models[7]. Among 43,097 UKB participants with complete 11-organ protein-derived age (ProAge) estimates, conventional ProAge deviation from the original ProAge framework represented overall protein-derived aging. Mean organ ProAge deviation and ProAge imbalance were calculated as the within-person mean and standard deviation of the 11 standardized organ ProAge deviations, respectively. As in the phenotype-derived analyses, mean organ ProAge deviation and ProAge imbalance were related but distinct (r=0.267, $P < 0.001$), ProAge imbalance correlated weakly with conventional ProAge deviation (r=0.130, $P < 0.001$), and median imbalance was higher in older age groups (**Fig. 6a,b**; **Supplementary Fig. 5**). After adjustment for conventional ProAge deviation, age and sex, higher ProAge imbalance was associated with mortality, all

six organ-disease endpoints and three multimorbidity transitions (HR range 1.16–1.40; **Fig. 6c**; **Supplementary Table 12**). Sensitivity analyses of covariate adjustment and imbalance construction generally supported these associations (**Supplementary Fig. 6a-d**), and HR estimates varied less between organ subsets as more organs were included (**Supplementary Fig. 6e**). ProAge imbalance also differentiated mortality within levels of conventional ProAge deviation: compared with Low/Low, Low/High and High/Low had intermediate estimates, whereas High/High had the largest estimate (overall log-rank $P = 2.82 \times 10^{-174}$; **Fig. 6d**); this ordering extended to disease and multimorbidity outcomes (**Supplementary Fig. 7**; **Supplementary Table 12**). In the common sample (n = 19,744), HR point estimates for both phenotype-derived and protein-derived imbalance were above 1 across these outcomes in models adjusted for age, sex and the corresponding mean organ AgeDev or mean organ ProAge deviation (**Fig. 6e; Supplementary Table 12**).

Discussion

Our findings highlight multi-organ aging imbalance as a complementary feature of biological aging relevant to health vulnerability. Using organ-age measures derived from routine physiological and biochemical biomarkers, we found that greater multi-organ imbalance was independently associated with mortality, incident organ disease, multimorbidity progression and frailty. Notably, higher imbalance was associated with elevated mortality risk even among individuals with relatively low overall biological aging. Mortality associations were supported by findings across five external cohorts, and analyses using protein-derived organ ages provided further support across measurement frameworks. Investigations of lifestyle, psychosocial, socioeconomic, and proteomic correlates also provided further insights into the characteristics and potential biological relevance of multi-organ aging imbalance.

Previous studies have characterized aging across multiple organ systems and linked organ-specific biological ages to disease and mortality[1,5]. Longitudinal multi-omic profiling has also identified distinct ageotypes, highlighting heterogeneity in the molecular pathways involved in aging[2]. More recent investigations have extended organ aging clocks across diverse populations and examined their associations with disease across organ systems and multimorbidity[6,8]. Building on these advances, our study extends the characterization of multi-organ aging beyond individual organ ages and specific aging patterns by quantifying the degree of divergence in aging across organs within individuals. The heterogeneous organ-aging profiles suggest that pronounced imbalance can arise from diverse combinations of organ-specific aging deviations, while the joint-stratification analyses indicate that this dispersion carries health-related information not fully reflected by overall biological-age deviation. Together, these findings highlight cross-organ dispersion as a complementary feature that enriches the characterization of individual aging profiles. Although incorporating imbalance improved model fit, the modest gains in risk discrimination suggest that its principal contribution lies in broadening our understanding of multi-organ aging rather than substantially improving individual risk prediction.

The associations of multi-organ aging imbalance with multimorbidity and frailty further highlight its

relevance to multisystem health vulnerability. Previous studies have linked proteomic aging to multimorbidity and frailty[9] and identified shared and pattern-specific biomarkers associated with multimorbidity[10]. Building on this evidence, our findings suggest that cross-organ aging dispersion may capture aspects of health vulnerability related to disease accumulation across organ systems, including among individuals without existing organ disease. Associations with frailty burden and incident frailty further extend this relevance beyond diagnosed diseases to broader health deficits. Differences in organ aging may reflect uneven physiological deterioration across systems, potentially contributing to variation in individuals' capacity to maintain health and function. This perspective may help explain why individuals with relatively low overall biological aging can nevertheless differ in their susceptibility to adverse health outcomes.

The associations of multi-organ aging imbalance with behavioural, psychosocial and socioeconomic factors suggest that cross-organ aging dispersion may be related to broader environmental and social circumstances. Previous large-scale exposome research has linked environmental exposures to biological aging and mortality[11]. Our findings extend this perspective to the distribution of aging across organ systems, suggesting that behavioural and social determinants may be relevant not only to the extent of biological aging but also to its heterogeneity across organs. Understanding these relationships may provide a basis for investigating how modifiable exposures and social conditions relate to differences in organ aging across populations.

Proteomic analyses provided molecular insights into multi-organ aging imbalance, highlighting pathways involved in metabolic regulation, immune signaling and cellular maintenance. Positive enrichment of amino acid and fatty acid metabolism, biological oxidation, and immune-effector and cytokine signaling, together with negative enrichment of telomere organization, DNA repair and cell-cycle pathways, were related to established hallmarks of aging, including altered metabolic regulation, inflammation, genomic instability and telomere biology[12]. These findings may be understood in the context of systemic influences on organ aging. Heterochronic parabiosis experiments have demonstrated that different tissues and cell types respond differently to a shared circulating environment, suggesting that tissue-specific sensitivity to systemic signals

may contribute to divergent aging trajectories across organs[13]. In addition, senescent cells can release inflammatory cytokines and other signaling molecules through the senescence-associated secretory phenotype (SASP), potentially influencing aging-related processes in distant tissues. Experimental evidence has shown that hepatocyte-specific senescence can induce senescence and dysfunction in extrahepatic organs through TGF-β signaling[14], illustrating how localized aging-related alterations may have systemic consequences. Together, these findings highlight metabolic and immune regulation, differential tissue responses to systemic signals, and interorgan communication as potentially interconnected processes relevant to multi-organ aging imbalance and its associations with health outcomes.

An important consideration is whether multi-organ aging imbalance captures meaningful variation in organ aging or primarily reflects extreme deviations in individual organs or the properties of the chosen dispersion measure. Several findings support the robustness of its associations with health outcomes. These associations were generally consistent across alternative definitions of imbalance and persisted after excluding organs with the most extreme age deviations. Analyses using different organ subsets and numbers also yielded broadly similar patterns, particularly for all-cause mortality. Moreover, extending the analysis from risk-based organ ages derived from routine clinical biomarkers to 11 protein-derived organ ages yielded broadly consistent findings, suggesting that the observed associations are not restricted to a single organ-age estimation framework. Together, these findings indicate that the prognostic relevance of multi-organ aging imbalance is not solely attributable to extreme organ-age deviations, a particular dispersion measure or a specific measurement framework. Nevertheless, differences in measurement precision and correlations among organ-age estimates may contribute to the observed dispersion, and further work is needed to distinguish biological heterogeneity from measurement-related variation.

This study has several strengths. The large population-based cohort enabled a comprehensive assessment of multi-organ aging imbalance across multiple health outcomes. Replication of mortality associations across five external cohorts, together with analyses using protein-derived organ ages and extensive sensitivity analyses, strengthened the robustness and generalizability of our findings. Several limitations still warrant consideration. First, the observational design precludes causal inference, and residual confounding cannot be

excluded despite adjustment for relevant covariates. Second, biomarker availability restricted organ coverage, particularly in external cohorts, and imbalance therefore describes dispersion among the measured systems. Where the complete UKB biomarker panel was unavailable, cohort-compatible models were reselected and retrained in UKB. External findings therefore support the imbalance framework across cohort-specific implementations, with more limited evidence for direct transport of the complete UKB models. Third, organ-age estimates at each assessment relied on a single set of biomarker measurements. Transient physiological variation and differences in measurement precision across organs may influence the estimated dispersion. Fourth, outcome ascertainment differed across cohorts, with some disease endpoints based on self-reported physician diagnoses. These differences may affect the comparability of cohort-specific association estimates. Finally, exposure and proteomic analyses were cross-sectional and confined to UKB, leaving their temporal relationships with imbalance and reproducibility across populations to be established.

In conclusion, our findings identify cross-organ aging dispersion as a complementary characteristic of biological aging associated with adverse health outcomes. Quantifying organ-age dispersion using routine clinical measurements provides a practical basis for investigating these associations in population cohorts. Evidence across populations and organ age measurement frameworks supports the relevance of this characteristic beyond conventional summaries of aging level. Considering both the extent of biological aging and its distribution across organs may provide a more comprehensive perspective on health vulnerability in individuals and populations.

Methods

Study design and participants

This multicohort observational study used UKB as the primary cohort to develop phenotype-derived organ biological ages and examine multi-organ aging imbalance in relation to health outcomes. UKB is a prospective population-based cohort in the United Kingdom[15]. Five external cohorts contributed replication and extension analyses. CHARLS and ELSA are nationally representative longitudinal studies of aging[16,17]. SSACB and TZL are prospective cohorts in suburban Shanghai and Taizhou, China, respectively[18–21]. NHANES is a nationally representative health and nutrition survey[22]. We used NHANES data from the 1999–2018 survey cycles. Characteristics of the study cohorts are summarized in **Supplementary Table 1**.

Of more than 500,000 UKB participants, 221,599 formed the phenotype-derived analysis population after exclusions for baseline cancer or pregnancy or incomplete data on candidate biomarkers (**Supplementary Fig. 8**). Baseline plasma protein data were available for a subset of UKB participants through the UK Biobank Pharma Proteomics Project, which used the Olink Explore 3072 proximity extension assay to measure 2,923 unique proteins[23]. After protein preprocessing, described below, and the same exclusions for baseline cancer or pregnancy, 43,097 participants formed the protein-derived analysis population.

Biomarker mapping and selection

UKB baseline routine clinical biomarkers were assigned a priori to cardiovascular, pulmonary, immune, renal, hepatic and metabolic systems, and biomarkers with absolute skewness greater than 1 were transformed using $\log(x + 1)$. The organ-specific candidate panels, the 42-biomarker cross-system candidate pool, variable definitions, units, derived measures and transformations are provided in **Supplementary Table 2**. UKB participants were randomly divided into a training set (70%; *n*=155,119) and a test set (30%; *n*=66,480), with the same split used for all six organ models and the overall model. Biomarker selection was performed in the training set using the R package *glmnet*[24]. For each organ, we fitted a Cox least absolute shrinkage and selection operator model for the corresponding incident organ-

disease outcome using chronological age, sex and the organ-specific candidate panel. The 42-biomarker overall candidate pool was evaluated in the same way using all-cause mortality. Selection stability was assessed in 50 full-size bootstrap samples drawn with replacement from the corresponding risk set within the training set. Within each sample, the penalty was chosen by tenfold cross-validation using $\alpha = 1$ and lambda.1se; a selection-frequency threshold of 95% was used to define stable biomarkers. Chronological age and sex contributed to selection but were not counted as biomarkers. The final biomarker panels for the six UKB organ models and the overall model are presented in **Fig. 2a** and **Supplementary Table 2**. Pairwise Pearson correlations among retained biomarkers were assessed in the fixed UKB training set (n = 155,119); all within-panel absolute correlations were below 0.70 (**Supplementary Fig. 9**).

The same six-system framework was adapted to the biomarker coverage of each external cohort. When all biomarkers in a final UKB panel were available, that panel was retained. Otherwise, the candidate panel was restricted to biomarkers meeting a relative coverage threshold of 80% across the required waves or survey cycles within the corresponding anthropometric or laboratory domain, and the same Cox LASSO procedure with 50 bootstrap samples was repeated in the fixed UKB training set. Albumin was retained in the SSACB hepatic panel for prespecified panel continuity (selection frequency, 70%). Cohort-compatible candidate and final biomarker panels are provided in **Supplementary Table 2**. Each cohort-compatible refit was additionally compared with its corresponding primary model in identical outcome-specific UKB test-set risk sets using age- and sex-adjusted Cox models, with AgeDev scores scaled using their respective UKB training data.

Construction of phenotype-derived biological ages and AgeDev

We constructed six organ-specific biological ages and an overall biological age in parallel in the UKB training set, fitting models separately in men and women. For each organ, chronological age (CA) and the retained organ-specific biomarkers were entered into a Gompertz proportional hazards model for the corresponding incident organ-disease outcome. The overall model used CA and the retained biomarkers to model all-cause mortality.

An age-only Gompertz model for the same outcome was fitted in the same sex-specific training sample to provide the reference for converting risk into biological age. The linear predictors for the full and age-only models were

$$\eta_1 = c_1 + \beta_1 CA + \sum_{j=1}^{p} \theta_j X_j, \qquad \eta_0(a) = c_0 + \beta_0 a,$$

where X_j denotes the jth retained biomarker and a is the age at which reference risk is evaluated. Biological age (BA) was defined as the age at which the age-only model produced the same cumulative risk over 10 years as the full model[3,25,26]:

$$BA = \frac{1}{\beta_0}\left[\eta_1 - c_0 + \log\left\{\frac{[\exp(\gamma_1 \tau) - 1]/\gamma_1}{[\exp(\gamma_0 \tau) - 1]/\gamma_0}\right\}\right], \qquad \tau = 10,$$

where γ_0 and γ_1 are the Gompertz shape parameters of the age-only and full models, respectively. The full derivation is provided in the **Supplementary Methods**. For each external cohort, models using the biomarker panel adapted to its available measurements were fitted separately in men and women in the UKB training set. The resulting equations were then applied to that cohort. Complete sex-specific operational equations for UKB and the external cohorts are provided in **Supplementary Table 2**.

For comparison, we trained elastic-net regression, linear support vector machine regression (SVM) and XGBoost models, three approaches commonly used in biomarker-based biological-age modelling[4,27]. They predicted CA from the same retained organ-specific biomarkers, used the same UKB training-test split and sex-specific framework, and were tuned by fivefold cross-validation in the training set. These models were implemented using the R packages *glmnet*, *LiblineaR* and *xgboost*, respectively.

Predicted ages from the primary and comparator models were converted to age deviations using the same procedure. For each measure, we fitted

$$\widehat{BA}_i = \alpha + \beta CA_i + \varepsilon_i$$

separately in men and women in the training set and defined

$$AgeDev_i = \widehat{BA}_i - (\hat{\alpha} + \hat{\beta} CA_i).$$

The training-set calibration coefficients were applied to the test set. For comparisons confined to the training and test sets, AgeDev measures were standardized using the training-set mean and sample s.d. Within each external cohort, predicted age was calibrated separately in men and women using a fixed sample with predicted age available for the relevant organ: ELSA wave 2, CHARLS wave 1, baseline in SSACB and TZL, and all eligible NHANES examinations. The corresponding calibration parameters for each cohort, organ and sex are provided in **Supplementary Table 2**. Standardization used fixed reference samples with complete organ panels.

UKB mortality, organ-disease and multimorbidity outcomes

The six UKB organ-disease composites represented cardiovascular, metabolic, kidney, liver, pulmonary and immune-related disease. They were defined from linked hospital diagnoses, baseline self-reports and cause-of-death records. Complete component definitions and International Classification of Diseases, Ninth and Tenth Revisions, codes are provided in **Supplementary Data 3**. Hospital diagnoses recorded on or before the baseline assessment and qualifying baseline self-reports defined prevalent disease. Clinical measurements and medications additionally informed baseline diabetes, hyperlipidaemia and chronic kidney disease. Diabetes was identified by glycated haemoglobin of at least 48 mmol mol^{-1}, glucose of at least 7.0 mmol l^{-1} or insulin use. Hyperlipidaemia was identified by cholesterol-lowering medication, and chronic kidney disease by an estimated glomerular filtration rate[28] below 60 ml min^{-1} per 1.73 m^2.

Participants with any prevalent component of a composite were excluded from its incident risk set. The first qualifying post-baseline hospital diagnosis or disease-specific death defined the incident event. Disease-specific deaths were identified by matching qualifying ICD-10 codes against any listed cause of death. Hospital-record follow-up ended on 30 October 2022 in England, 31 August 2022 in Scotland and 31 May 2022 in Wales. Death-record follow-up ended on 31 October 2022 in England, 31 July 2021 in Scotland and

28 February 2018 in Wales. Participants without an event were followed until the applicable hospital-record end date or an earlier death from another cause.

We derived three transitions across the six disease domains. These were no disease at baseline to a first incident disease, no disease to a second distinct disease, and one baseline disease to the first additional disease. Baseline was the time origin for all three transitions. Event time was the date of the first or second distinct disease, as applicable. Two distinct diseases first recorded on the same day could contribute to the second-disease endpoint. Participants without the required transition were censored at the earliest censoring time across the six disease domains. All-cause mortality was ascertained from linked death records through the country-specific death-record end dates given above.

External-cohort mortality and organ-disease outcomes

External disease definitions were adapted to the available records in each cohort; cohort-specific endpoint definitions and harmonization details are provided in **Supplementary Data 3**. SSACB and TZL supplied cardiovascular, metabolic, kidney, liver and pulmonary outcomes from diagnosis and cause-of-death records mapped to the corresponding UKB components. Their organ-age panels comprised cardiovascular, metabolic, kidney and liver systems, so pulmonary disease contributed only as an outcome of the four-organ imbalance measure and not as a matched pulmonary AgeDev outcome. Baseline diagnoses and self-reported histories defined prevalent disease, with glycated haemoglobin and glucose additionally used to identify baseline diabetes in SSACB and glucose used in TZL. The first qualifying post-baseline diagnosis or disease-specific death defined the incident event. Follow-up continued through 31 December 2024 in SSACB and 31 December 2021 in TZL, with an earlier death from another cause treated as censoring.

ELSA evaluated cardiovascular disease as heart disease or stroke, pulmonary disease as chronic lung disease and metabolic disease as diabetes or high cholesterol. CHARLS evaluated cardiovascular disease as heart disease or stroke, kidney disease as self-reported kidney disease and metabolic disease as diabetes or dyslipidaemia. Available glycated haemoglobin, glucose and medication data supplemented the baseline metabolic definitions, and estimated glomerular filtration rate supplemented the CHARLS baseline kidney

definition. Disease follow-up began at ELSA wave 4 (2008–2009) and CHARLS wave 1 (2011–2012), with incident diagnoses identified through ELSA wave 9 (2018–2019) and CHARLS wave 4 (2018), respectively. The event was the first subsequent report of the relevant physician diagnosis; participants without an event were censored at the last visit with known disease status.

All-cause mortality follow-up in SSACB and TZL used recorded death dates and the administrative end dates specified above. For NHANES, all-cause mortality was ascertained through National Death Index linkage using the National Center for Health Statistics 2019 public-use linked mortality files; follow-up ran from interview to death or 31 December 2019[29]. ELSA mortality follow-up extended from wave 4 to wave 6 (2012–2013), and CHARLS mortality follow-up from wave 1 to wave 4. In ELSA and CHARLS, event time was approximated by the midpoint between the last visit confirming survival and the first visit window reporting death; non-events were censored at the last confirmed-alive visit.

Frailty outcomes in ELSA and CHARLS

Frailty was assessed using deficit-accumulation indices[30]. The ELSA adapted index contained 60 items and was calculated when at least 30 were observed[31]. The CHARLS index was adapted from published deficit-accumulation approaches[32,33] and contained 39 items, with at least 80% required to be observed. Component deficits and scoring rules are provided in **Supplementary Data 3**. Frailty burden was analysed as a repeated continuous measure at ELSA waves 2 (2004–2005), 4 and 6 and CHARLS waves 1 and 3 (2015).

Incident-frailty risk sets were initiated at the same waves among participants with a frailty index below 0.25. Participants were followed through later frailty assessments up to ELSA wave 9 or CHARLS wave 5 (2020). The event was the first index value of at least 0.25; participants without an event were censored at their last assessment with a calculable index. A threshold of 0.21 was examined in both cohorts as a sensitivity analysis.

Evaluation of phenotype-derived biological ages

Agreement between predicted biological age and CA was evaluated in the UKB training and test sets using

Pearson correlation and mean absolute error; the corresponding estimates are provided in **Supplementary Table 2**. Partial correlations among the six primary organ AgeDev measures and overall AgeDev were estimated in the test set after adjustment for CA and sex.

We first related each AgeDev measure separately to incident organ disease using Cox models adjusted for CA and sex. To assess conditional organ specificity, all six organ AgeDev measures and overall AgeDev were entered simultaneously into each organ-disease model with CA and sex. Robustness was evaluated by adding ethnicity, smoking, alcohol consumption and education. The base and extended models used the same outcome-specific complete-case samples. We also compared age- and sex-adjusted matched organ-disease estimates between the training and test sets. Using the same test participants eligible for each outcome, primary estimates were compared descriptively with elastic net, SVM and XGBoost estimates. PhenoAge deviation[3] and matched protein-derived organ AgeDev measures were each evaluated in separate Cox models adjusted for CA and sex. Hazard ratios were reported per 1-s.d. higher AgeDev.

External-cohort analyses related each available organ AgeDev to its matched cohort-specific disease outcome using Cox models adjusted for CA and sex. Cardiovascular, metabolic, renal, hepatic and pulmonary pairs were evaluated. Immune AgeDev was excluded because no comparable external endpoint was available. When at least two comparable cohort estimates were available, including the UKB test-set estimate, log hazard ratios were combined using restricted maximum-likelihood random-effects meta-analysis using the R package *metafor*[34]. Hartung–Knapp confidence intervals were used for at least three estimates, and z-based confidence intervals for two. We report the pooled hazard ratio, 95% confidence interval, τ^2, I^2 and number of contributing cohorts. Cohort-specific estimates remained the primary presentation. NHANES provided a complementary prognostic evaluation by relating each organ AgeDev to all-cause mortality using Cox models adjusted for CA and sex.

Construction of multi-organ imbalance

For the primary UKB multi-organ analyses, the six organ AgeDev measures were standardized using their means and sample s.d. in the full 221,599-participant phenotype-derived population. If μ_o and σ_o denote

these parameters for organ o, the standardized value for participant i was

$$Z_{io} = \frac{AgeDev_{io} - \mu_o}{\sigma_o}.$$

All six measures were required in UKB. With $K = 6$, mean organ AgeDev and multi-organ imbalance were calculated as

$$\text{mean}_i = \frac{1}{K}\sum_{o=1}^{K} Z_{io}\,, \qquad \text{imbalance}_i = \sqrt{\frac{1}{K-1}\sum_{o=1}^{K}(Z_{io} - \text{mean}_i)^2}.$$

Mean organ AgeDev summarized the average deviation across organs, whereas imbalance quantified the dispersion of these deviations within an individual. Mean organ AgeDev, multi-organ imbalance and overall AgeDev were each subsequently standardized to a mean of zero and an s.d. of one in the same 221,599-participant population for downstream analyses. External organ AgeDev measures were standardized using cohort-specific reference samples. These comprised participants with complete organ panels at baseline in SSACB and TZL, ELSA wave 2 and CHARLS wave 1, and eligible NHANES participants with complete six-organ data drawn from the 1999–2018 surveys. These parameters were applied to subsequent waves and outcome analyses. Cohort-specific mean organ AgeDev and imbalance were then calculated from the organ systems available in each cohort. Both measures were subsequently standardized using the corresponding reference sample, with these parameters held fixed for subsequent waves and outcome analyses.

Evaluation of multi-organ imbalance

We summarized imbalance across four CA groups (<50, 50–59, 60–69 and ≥70 years) and by sex in the UKB population and each external reference sample. Age groups were compared using Kruskal–Wallis tests and women and men using Wilcoxon rank-sum tests. Age and sex comparisons were treated as separate families, with Benjamini–Hochberg correction[35] across cohorts within each family. Longitudinal analyses used ELSA wave 2 with waves 4 and 6 and CHARLS wave 1 with wave 3. Paired changes from baseline

were summarized with *t*-based 95% confidence intervals. Annual change was estimated using participant fixed-effects models with actual follow-up time and participant-clustered robust standard errors.

In UKB, separate Cox models related multi-organ imbalance to all-cause mortality, the six organ-disease composites and the three multimorbidity transitions. Estimates were expressed per 1-s.d. higher imbalance. The primary model included overall AgeDev, CA and sex. A reduced model included only CA and sex, whereas a parallel model replaced overall AgeDev with mean organ AgeDev. For each organ-disease outcome, another model added the corresponding organ AgeDev to the primary adjustment set. The expanded model added ethnicity, assessment centre, the first ten genetic principal components, Townsend deprivation, education, household income, physical activity, sedentary behaviour, diet, smoking, alcohol consumption and sleep. In multivariable risk-factor models, missing continuous covariates were median-imputed with missingness indicators, and categorical covariates included a missing category. Cause-specific Cox models were primary for organ-disease outcomes. Fine–Gray models[36] with the same covariates were fitted as a competing-risk sensitivity analysis.

External mortality and disease models included multi-organ imbalance, mean organ AgeDev, CA and sex. Frailty burden was analysed at ELSA waves 2, 4 and 6 and CHARLS waves 1 and 3 using Gaussian identity-link generalized estimating equations implemented using the R package *geepack*[37], with an exchangeable working correlation and participant-clustered robust standard errors. Coefficients represented the difference in frailty-index percentage points per 1-s.d. higher imbalance. Incident frailty was analysed using repeated-landmark Cox models with the same covariates, stratification by landmark wave and participant-clustered robust standard errors.

Five alternative dispersion measures were examined: the range, mean absolute deviation from the within-person organ mean, interquartile range, top-two versus bottom-two mean difference and coefficient of variation across the six reconstructed organ biological ages. We also recalculated imbalance after centring each organ AgeDev on its median and scaling it by its median absolute deviation. Further analyses restricted participants to the middle 80% of the primary imbalance distribution. Organ-exclusion analyses removed the

outcome-matched organ, the organ with the largest absolute deviation from the participant's six-organ mean, or both the highest and lowest organ values. We also evaluated every possible three-, four- and five-organ subset. Mean organ AgeDev and imbalance were reconstructed together whenever the organ set or standardization changed. Alternative-metric models included both mean organ AgeDev and overall AgeDev; central-range models included overall AgeDev, and organ-exclusion and subset models included the corresponding mean organ AgeDev. All models included CA and sex.

To quantify incremental prognostic information, we fitted three nested Cox models in the same endpoint-specific sample. The reference model contained CA, sex, ethnicity, assessment centre, the first ten genetic principal components, Townsend deprivation, education and household income. It also included physical activity, sedentary behaviour, diet, smoking, alcohol consumption, sleep, loneliness, psychological distress and neuroticism. The second model added the 18-marker overall AgeDev, and the third added multi-organ imbalance. The primary incremental contrast for imbalance was the third model versus the second. Model fit was compared using likelihood-ratio tests. Apparent discrimination was summarized using Harrell's C-index[38] and its between-model difference, without optimism correction.

Imbalance-tail profiles and joint risk strata

The 10th and 90th percentiles of multi-organ imbalance in the 221,599-participant UKB population defined the bottom decile, middle 80% and top decile. K-means clustering was applied separately to the six organ AgeDev z-scores in the two tails. In the top decile, the primary gap-statistic one-standard-error rule[39] favoured a single cluster. Silhouette and subsampling-stability diagnostics favoured six clusters (mean silhouette, 0.210; mean adjusted Rand index, 0.964); we used this solution to define profiles T1–T6. Data-driven diagnostics selected $k = 1$ in the bottom decile, where organ patterns were largely concordant. We nevertheless fixed $k = 2$ to obtain two descriptive burden profiles (B1–B2) for comparison. Cox models related profiles to mortality, organ disease and multimorbidity, using the middle 80% as reference and adjusting for overall AgeDev, CA and sex.

To test whether imbalance differentiated risk within levels of overall ageing, overall AgeDev and imbalance

were divided at their respective UKB population medians to define Low/Low, Low/High, High/Low and High/High strata. Cox models for the same ten outcomes used Low/Low as the reference and adjusted for CA and sex; unadjusted mortality curves and 13-year cumulative mortality were estimated by the Kaplan–Meier method. External frailty analyses used the same four-group structure with mean organ AgeDev as the ageing-level dimension. Cohort-specific medians were estimated at ELSA wave 2 and CHARLS wave 1 and applied at later landmarks. Incident-frailty models used Low/Low as the reference, adjusted for CA and sex, were stratified by landmark wave and used participant-clustered robust standard errors.

Exposure associations with multi-organ imbalance

We examined 21 behavioral, dietary, sleep, psychosocial and socioeconomic indicators in separate cross-sectional models of UKB multi-organ imbalance. The dietary indicators were the six components of the adapted Mediterranean-style diet score used in our initial analysis: fruit, vegetables, fish, red meat, processed meat and wholegrain choice. The fruit, vegetable, fish, red-meat and processed-meat definitions and thresholds followed a previously published UKB healthy diet score[40]. Wholegrain choice captured grain quality, a dietary dimension included in other UKB healthy diet assessments; in our analysis, it was defined using participants' reported bread and cereal types[41]. The other indicators were non-current smoking; alcohol intake of no more than 14 units per week among current drinkers; higher physical activity; less sedentary behavior; five sleep characteristics from a published healthy sleep score—early chronotype, 7–8 h of sleep, no frequent insomnia, no snoring and no frequent daytime sleepiness[42]; lower neuroticism; absence of loneliness; lower psychological distress; university education; lower Townsend deprivation; and higher household income. Exact fields, thresholds and coding are provided in **Supplementary Table 10**.

Indicators were coded in favorable directions. Continuous indicators were analyzed per 1 s.d. increase, and binary indicators as 1 versus 0. Lower neuroticism was represented by a reverse-coded continuous z-score. Alcohol-amount analyses were restricted to current drinkers. Household income was analyzed as a five-level ordinal trend per 1 s.d.

Each indicator was analyzed separately, without mutual adjustment. The base linear model included age and sex; the conditional model additionally included 18-marker overall AgeDev. Each analysis used exposure-specific complete cases, with no imputation of the exposure. Continuous indicators were standardized within their eligible samples, and the same standardization was used in both models. We used HC3 robust standard errors and applied the Benjamini–Hochberg procedure separately to the 21 tests in each adjustment model. These associations were interpreted as observational correlates.

Proteomic associations and pathway enrichment

We excluded participants with more than 1,000 missing protein measurements and proteins with more than 10% missingness, retaining 44,831 participants and 2,916 proteins. Remaining values were imputed using k-nearest neighbours ($k = 10$)[43]. Each protein was standardized in the 43,097-participant protein-derived population. Among the 19,744 participants who also belonged to the phenotype-derived population, standardized protein abundance was regressed on phenotype-derived multi-organ imbalance, adjusting for overall AgeDev, CA, sex and body mass index. Benjamini–Hochberg correction was applied across all 2,916 proteins.

For gene set enrichment analysis[44], all proteins were ranked by the signed *t* statistic for imbalance without significance-based prefiltering. We used the fgseaMultilevel function in the R package *fgsea*[45] with 10,000 simple permutations and gene sets containing 10–500 measured proteins from Hallmark[46], Reactome, Gene Ontology Biological Process, KEGG legacy and KEGG medicus in MSigDB v2024.1.Hs[47]. Benjamini–Hochberg correction was applied separately within Hallmark, Reactome, Gene Ontology Biological Process and the combined KEGG family. Significant pathways with positive and negative normalized enrichment scores were grouped separately using MAPA[48]. Pathways were connected when the Jaccard similarity of their leading-edge proteins was at least 0.25 or the token-based Jaccard similarity of their normalized labels was at least 0.40. Modules containing multiple pathways were labelled by the pathway with the lowest false discovery rate within the corresponding database family.

Protein-derived multi-organ imbalance and comparisons with phenotype-derived measures

We applied the published ProAge models to derive predicted ages for adipose tissue, artery, brain, heart, immune tissue, intestine, kidney, liver, lung, muscle and pancreas, together with conventional and organismal ProAge measures[7]. Within the 43,097-participant protein-derived population, each predicted ProAge was regressed on CA separately in men and women; the residual defined ProAge deviation. Sex-specific residuals were combined and each measure was standardized in the full population. Conventional ProAge deviation served as the overall protein-age comparator. Mean organ ProAge deviation was the arithmetic mean of the 11 standardized organ deviations, and ProAge imbalance was their within-person sample s.d.; both were standardized in the same population.

ProAge imbalance was summarized across CA, sex and race or ethnicity groups. Cox models related it to all-cause mortality, the six organ-disease outcomes and the three multimorbidity transitions, with adjustment for conventional ProAge deviation, CA and sex. Robustness analyses replaced or augmented conventional ProAge deviation with organismal, mean organ or outcome-matched organ ProAge deviation or with Townsend deprivation, education, household income, physical activity, sedentary behaviour, diet, smoking, alcohol consumption and sleep. Alternative metric, standardization, central-range, organ-exclusion and three- to ten-organ subset analyses followed the phenotype-derived framework. Alternative-metric models included mean organ ProAge deviation and conventional ProAge deviation; central-range models included conventional ProAge deviation, and organ-exclusion and subset models included the corresponding mean organ ProAge deviation. All models included CA and sex.

Joint strata were defined using the population medians of conventional ProAge deviation and ProAge imbalance, following the phenotype-derived analysis. Cox models for the same ten outcomes used Low/Low as the reference and adjusted for CA and sex; mortality was additionally summarized using Kaplan–Meier curves.

Comparisons between phenotype- and protein-derived measures included the 19,744 participants with both

measurements. Phenotype-derived and ProAge measures retained their respective reference scales established in 221,599 and 43,097 participants. Agreement was quantified using Pearson correlations, with Spearman correlations as sensitivity analyses. For each outcome, the two imbalance measures were analysed on identical participant rows in separate Cox models. The phenotype model adjusted for mean organ AgeDev, CA and sex, and the protein model for mean organ ProAge deviation, CA and sex.

Statistical analysis

All statistical tests were two-sided, and 95% confidence intervals are reported. Cox models were fitted using the R package *survival*, with Efron's method for ties. Where multiple-testing correction was specified, Benjamini–Hochberg correction was applied within each analysis-specific testing family rather than across all analyses.

Declarations

Ethics approval and consent to participate

This study used data from UK Biobank (UKB), the China Health and Retirement Longitudinal Study (CHARLS), the English Longitudinal Study of Ageing (ELSA), the Shanghai Suburban Adult Cohort and Biobank (SSACB), the Taizhou Longitudinal Study (TZL) and the US National Health and Nutrition Examination Survey (NHANES). The contributing cohorts obtained ethics approvals and informed consent under their original study protocols.

UKB has research tissue bank approval from the North West Multi-centre Research Ethics Committee. This research used the UK Biobank Resource under Application Number [92718]. CHARLS was approved by the Institutional Review Board of Peking University (IRB00001052-11015 for the household survey and physical measurements, and IRB00001052-11014 for biomarker collection). ELSA received approval from the London Multi-Centre Research Ethics Committee for the early waves and from the relevant UK research ethics committees for subsequent waves. Participants in CHARLS and ELSA provided informed consent. SSACB was approved by the ethical review board of the School of Public Health of Fudan University (2016-04-0586). TZL was approved by the Human Ethics Committee of Fudan University and the Ethics Committee of Fudan University Taizhou Institute of Health Sciences (085 and B018, respectively), and participants provided written informed consent[21]. NHANES protocols were approved by the National Center for Health Statistics ethics review board, and all participants provided written informed consent.

Data availability

UKB data are available to approved researchers through its application process (https://www.ukbiobank.ac.uk/use-our-data/apply-for-access/). CHARLS data and documentation are available through the study data portal following registration (https://charls.pku.edu.cn/en/). ELSA data are available through the UK Data Service under the applicable access conditions (https://www.elsa-project.ac.uk/accessing-elsa-data). NHANES public-use data are available from the US Centers for Disease Control and Prevention (https://www.cdc.gov/nchs/nhanes/), and the 2019 public-use linked mortality files are available through the National Center for Health Statistics linked-data programme (https://www.cdc.gov/nchs/linked-data/mortality-files/).

SSACB and TZL data are available from the corresponding authors upon reasonable request, subject to the respective cohorts' data-access requirements.

Code availability

Analyses were conducted in R (version 4.4.1) using publicly available R packages, including survival, glmnet, flexsurv, cmprsk, geepack, metafor, sandwich, cluster, fgsea, impute, LiblineaR and xgboost. The analysis code will be made publicly available upon publication of this article.

Funding

This work was supported by the National Key Research and Development Program of China (2023YFC3606300 and 2024YFC3405800), the National Natural Science Foundation of China (82304239), Noncommunicable Chronic Diseases-National Science and Technology Major Project (2023ZD0510000), and 'Shuguang Program' supported by Shanghai Education Development Foundation and Shanghai Municipal Education Commission (23SG02).

Author contributions

Yucan Li, Kelin Xu and Xingdong Chen conceived and designed the study. Yucan Li performed the analyses and drafted the manuscript. Xinming Xu, Xinyi He and Yi Zheng contributed to the methodology and interpretation of the results. Chen Suo, Zhenqiu Liu, Ziyu Yuan and Yanfeng Jiang contributed to data curation and interpretation of the findings. Kelin Xu and Xingdong Chen supervised the study. All authors critically revised the manuscript and approved the final version.

Competing interests

The authors declare no competing interests.

Acknowledgements

We thank the participants, investigators and staff of UKB, CHARLS, ELSA, SSACB, TZL and NHANES for their contributions to the cohort resources used in this study.

References

1. Tian, Y. E. *et al.* Heterogeneous aging across multiple organ systems and prediction of chronic disease and mortality. *Nat. Med.* **29**, 1221–1231 (2023).
2. Ahadi, S. *et al.* Personal aging markers and ageotypes revealed by deep longitudinal profiling. *Nat. Med.* **26**, 83–90 (2020).
3. Levine, M. E. *et al.* An epigenetic biomarker of aging for lifespan and healthspan. *Aging* **10**, 573–591 (2018).
4. Bortz, J. *et al.* Biological age estimation using circulating blood biomarkers. *Commun. Biol.* **6**, 1089 (2023).
5. Oh, H. S.-H. *et al.* Organ aging signatures in the plasma proteome track health and disease. *Nature* **624**, 164–172 (2023).
6. Kivimäki, M. *et al.* Proteomic organ-specific ageing signatures and 20-year risk of age-related diseases: the whitehall II observational cohort study. *Lancet Digit. Health* **7**, e195–e204 (2025).
7. Oh, H. S.-H. *et al.* Plasma proteomics links brain and immune system aging with healthspan and longevity. *Nat. Med.* **31**, 2703–2711 (2025).
8. Wang, Y. *et al.* Organ-specific proteomic aging clocks predict disease and longevity across diverse populations. *Nat. Aging* **6**, 162–180 (2026).
9. Argentieri, M. A. *et al.* Proteomic aging clock predicts mortality and risk of common age-related diseases in diverse populations. *Nat. Med.* **30**, 2450–2460 (2024).
10. Ornago, A. M. *et al.* Shared and specific blood biomarkers for multimorbidity. *Nat. Med.* **32**, 736–745 (2026).
11. Argentieri, M. A. *et al.* Integrating the environmental and genetic architectures of aging and mortality. *Nat. Med.* **31**, 1016–1025 (2025).
12. López-Otín, C., Blasco, M. A., Partridge, L., Serrano, M. & Kroemer, G. Hallmarks of aging: an expanding universe. *Cell* **186**, 243–278 (2023).
13. Pálovics, R. *et al.* Molecular hallmarks of heterochronic parabiosis at single-cell resolution. *Nature* **603**, 309–314 (2022).
14. Kiourtis, C. *et al.* Hepatocellular senescence induces multi-organ senescence and dysfunction via TGFβ. *Nat. Cell Biol.* **26**, 2075–2083 (2024).
15. Sudlow, C. *et al.* UK biobank: an open access resource for identifying the causes of a wide range of complex diseases of middle and old age. *PLoS Med.* **12**, e1001779 (2015).
16. Zhao, Y., Hu, Y., Smith, J. P., Strauss, J. & Yang, G. Cohort profile: the China health and retirement longitudinal study (CHARLS). *Int. J. Epidemiol.* **43**, 61–68 (2014).
17. Steptoe, A., Breeze, E., Banks, J. & Nazroo, J. Cohort profile: the english longitudinal study of ageing. *Int. J. Epidemiol.* **42**, 1640–1648 (2013).
18. Zhao, Q. *et al.* Cohort profile: protocol and baseline survey for the Shanghai suburban adult cohort and biobank (SSACB) study. *BMJ Open* **10**, e035430 (2020).
19. Zhao, Q. *et al.* Establishment of Shanghai suburban adult cohort and biobank. *Chin. J. Epidemiol.* **44**, 28–33 (2023).
20. Wang, X. *et al.* Rationales, design and recruitment of the Taizhou Longitudinal Study. *BMC Public Health* **9**, 223 (2009).
21. Jiang, Y. *et al.* The taizhou longitudinal study: a population-based biobank resource of genetic and biochemical biomarkers for precision medicine in China. *J. Genet. Genomics* **53**, 1283–1291 (2026).
22. Zipf, G. *et al. National Health and Nutrition Examination Survey: Plan and Operations, 1999–2010*. 1–37 https://www.cdc.gov/nchs/data/series/sr_01/sr01_056.pdf (2013).
23. Sun, B. B. *et al.* Plasma proteomic associations with genetics and health in the UK biobank. *Nature* **622**, 329–338 (2023).
24. Simon, N., Friedman, J., Hastie, T. & Tibshirani, R. Regularization paths for cox's proportional hazards model via coordinate descent. *J. Stat. Softw.* **39**, 1–13 (2011).
25. Li, Y. *et al.* CardioMetAge estimates cardiometabolic aging and predicts disease outcomes. *BMC Med.* **24**, 129 (2026).

26. Li, Y. *et al.* Effect of caloric restriction on organ-specific biological aging in a randomized clinical trial. *Clin. Nutr.* **60**, 106625 (2026).
27. Bae, C.-Y. *et al.* Comparison of biological age prediction models using clinical biomarkers commonly measured in clinical practice settings: AI techniques vs. Traditional statistical methods. *Front. Anal. Sci.* **1**, 709589 (2021).
28. Inker, L. A. *et al.* New creatinine- and cystatin C–based equations to estimate GFR without race. *N. Engl. J. Med.* **385**, 1737–1749 (2021).
29. National Center For Health Statistics. *The Linkage of National Center for Health Statistics Survey Data to the National Death Index – 2019 Linked Mortality File (LMF): Linkage Methodology and Analytic Considerations*. https://www.cdc.gov/nchs/data/datalinkage/2019ndi-linkage-methods-and-analytic-considerations-508.pdf (2022).
30. Searle, S. D., Mitnitski, A., Gahbauer, E. A., Gill, T. M. & Rockwood, K. A standard procedure for creating a frailty index. *BMC Geriatr.* **8**, 24 (2008).
31. Marshall, A., Nazroo, J., Tampubolon, G. & Vanhoutte, B. Cohort differences in the levels and trajectories of frailty among older people in England. *J. Epidemiol. Community Health* **69**, 316–321 (2015).
32. Zhang, K. *et al.* Association of childhood and adulthood socioeconomic status with frailty index trajectories: using five-wave panel data from the China health and retirement longitudinal study (CHARLS). *Arch. Gerontol. Geriatr.* **131**, 105780 (2025).
33. Li, C. *et al.* Association of Cystatin C Kidney Function Measures With Long-term Deficit-Accumulation Frailty Trajectories and Physical Function Decline. *JAMA Netw. Open* **5**, e2234208 (2022).
34. Viechtbauer, W. Conducting meta-analyses in R with the metafor package. *J. Stat. Softw.* **36**, 1–48 (2010).
35. Benjamini, Y. & Hochberg, Y. Controlling the false discovery rate: a practical and powerful approach to multiple testing. *J. R. Stat. Soc. Ser. B Stat. Methodol.* **57**, 289–300 (1995).
36. Fine, J. P. & Gray, R. J. A proportional hazards model for the subdistribution of a competing risk. *J. Am. Stat. Assoc.* **94**, 496–509 (1999).
37. Halekoh, U., Højsgaard, S. & Yan, J. The R package geepack for generalized estimating equations. *J. Stat. Softw.* **15**, 1–11 (2006).
38. Harrell, F. E., Jr., Califf, R. M., Pryor, D. B., Lee, K. L. & Rosati, R. A. Evaluating the yield of medical tests. *JAMA J. Am. Med. Assoc.* **247**, 2543–2546 (1982).
39. Tibshirani, R., Walther, G. & Hastie, T. Estimating the number of clusters in a data set via the gap statistic. *J. R. Stat. Soc. Ser. B Stat. Methodol.* **63**, 411–423 (2001).
40. Tang, R. *et al.* Self-reported frequency of adding salt to food and risk of incident chronic kidney disease. *JAMA Netw. Open* **6**, e2349930 (2023).
41. Liu, W., Wang, T., Zhu, M. & Jin, G. Healthy diet, polygenic risk score, and upper gastrointestinal cancer risk: a prospective study from UK biobank. *Nutrients* **15**, 1344 (2023).
42. Fan, M. *et al.* Sleep patterns, genetic susceptibility, and incident cardiovascular disease: a prospective study of 385 292 UK biobank participants. *Eur. Heart J.* **41**, 1182–1189 (2020).
43. Troyanskaya, O. *et al.* Missing value estimation methods for DNA microarrays. *Bioinformatics* **17**, 520–525 (2001).
44. Subramanian, A. *et al.* Gene set enrichment analysis: a knowledge-based approach for interpreting genome-wide expression profiles. *Proc. Natl. Acad. Sci.* **102**, 15545–15550 (2005).
45. Korotkevich, G. *et al.* Fast gene set enrichment analysis. Preprint at https://doi.org/10.1101/060012 (2021).
46. Liberzon, A. *et al.* The molecular signatures database hallmark gene set collection. *Cell Syst.* **1**, 417–425 (2015).
47. Liberzon, A. *et al.* Molecular signatures database (MSigDB) 3.0. *Bioinformatics* **27**, 1739–1740 (2011).
48. Ge, Y. *et al.* Leveraging large language models for redundancy-aware pathway analysis and deep biological interpretation. Preprint at https://doi.org/10.1101/2025.08.23.671949 (2025).

Figure legends

Fig. 1

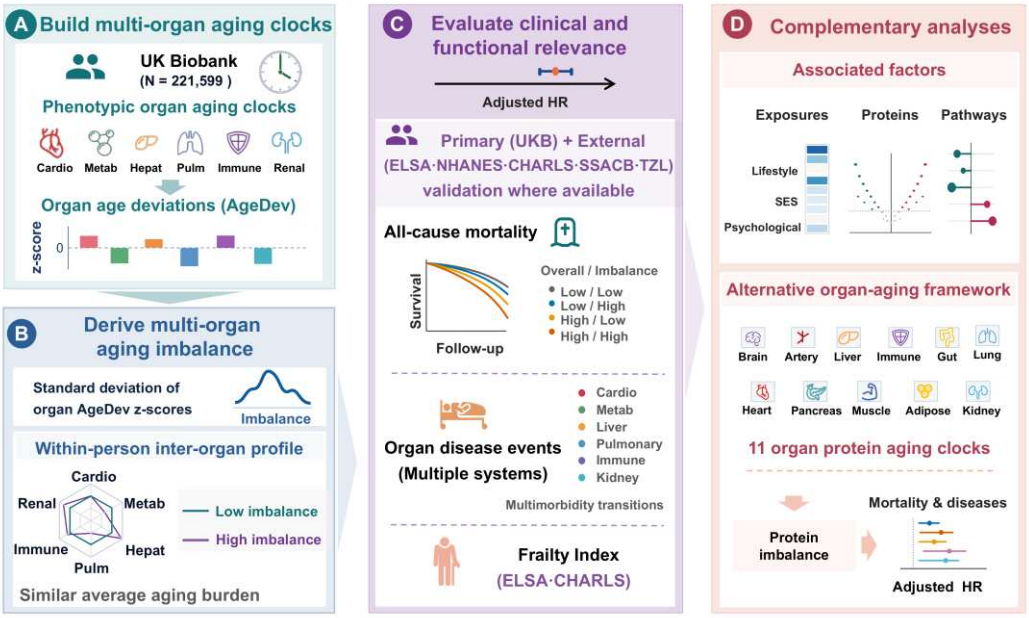


Fig. 1 | Study framework for multi-organ aging imbalance. a, Construction of cardiovascular, metabolic, hepatic, pulmonary, immune and renal phenotype-derived organ aging clocks and their age-calibrated organ age-deviation (AgeDev) measures in 221,599 UK Biobank (UKB) participants. **b,** Derivation of multi-organ imbalance as the within-person sample standard deviation of the six standardized organ AgeDev values. The schematic profiles illustrate that similar average organ-aging burden can coexist with low or high inter-organ dispersion. **c,** Evaluation of clinical and functional relevance across all-cause mortality, organ-disease events, multimorbidity transitions and frailty. UKB provided the primary analyses; ELSA, NHANES, CHARLS, SSACB and TZL contributed external analyses where data were available, and ELSA and CHARLS additionally contributed frailty outcomes. The mortality schematic previews joint overall AgeDev and imbalance strata. **d,** Complementary analyses of associated exposures, proteins and pathways and extension to an alternative framework comprising 11 protein-derived organ ages, their corresponding age deviations and protein-derived imbalance. CHARLS, China Health and Retirement Longitudinal Study; ELSA, English Longitudinal Study of Ageing; HR, hazard ratio; NHANES, National Health and Nutrition Examination Survey; SES, socioeconomic status; SSACB, Shanghai Suburban Adult Cohort and Biobank; TZL, Taizhou Longitudinal Study.

Fig. 2

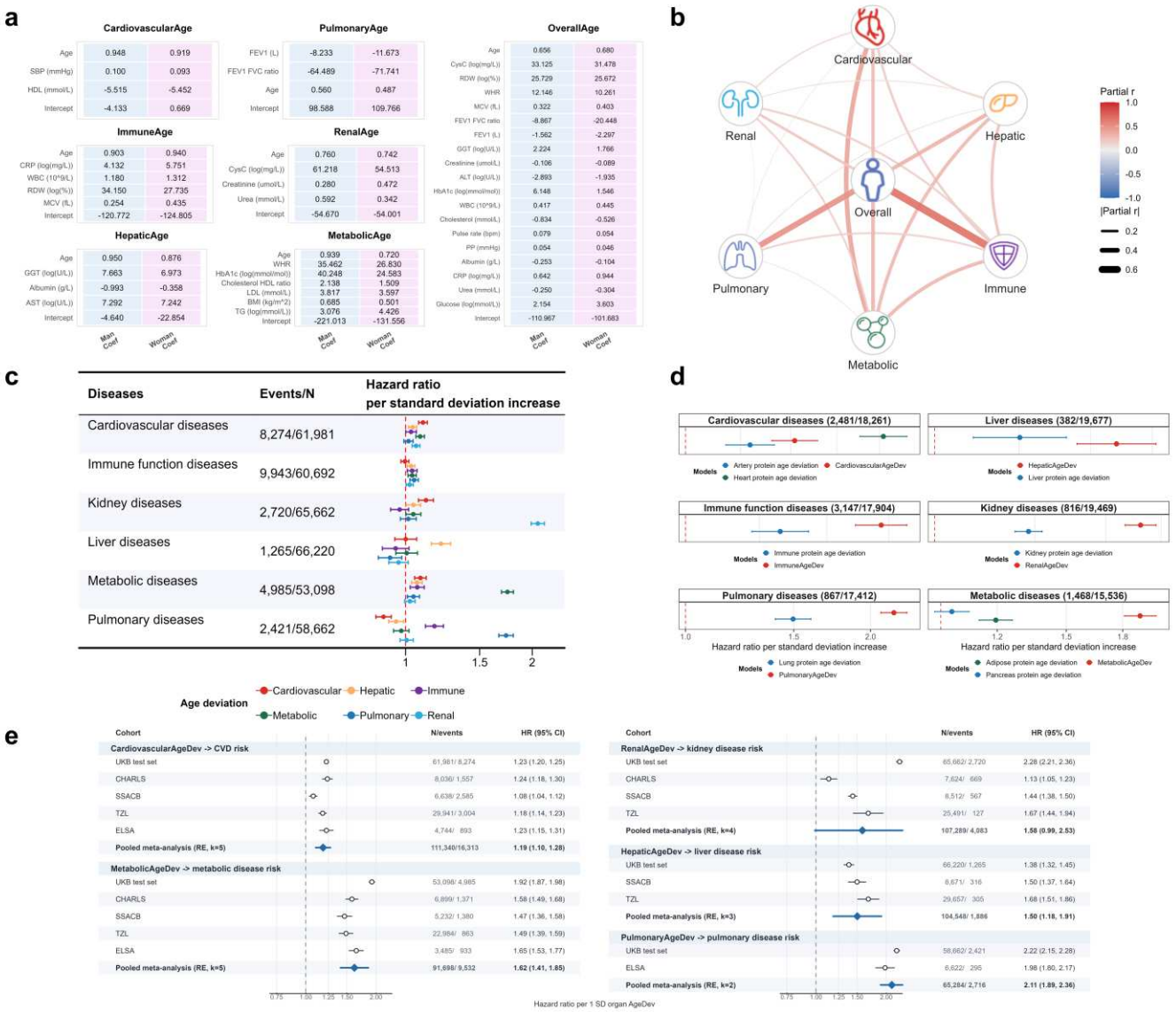


Fig. 2 | Routine clinical biomarkers yield phenotype-derived biological ages across organ systems. a, Final cardiovascular, pulmonary, immune, renal, hepatic, metabolic and overall biological-age equations. The columns for men and women give the operational coefficients used to calculate biological age in the final sex-specific equations. **b,** Partial-correlation network among the six organ AgeDev measures and overall AgeDev in the UKB test set (n = 66,480), adjusted for chronological age and sex. Edge width represents the absolute partial correlation and edge colour its direction and magnitude. **c,** Associations of all six organ AgeDev measures with each matched incident organ-disease outcome in the test set. Cox models included all six organ AgeDev measures and overall AgeDev simultaneously, with chronological age and sex as covariates; estimates are reported per 1-s.d. higher AgeDev. **d,** Separate age- and sex-adjusted associations of matched phenotype-derived and protein-derived organ AgeDev measures with incident organ disease among participants in the phenotype-protein common sample (n = 19,744). **e,** Cohort-specific and pooled associations between organ AgeDev and matched organ-disease outcomes. UKB estimates are from the test set; external estimates are shown where comparable data were available. Random-effects meta-analyses were performed when at least two cohort estimates were available. Points denote hazard ratios (HRs), horizontal bars 95% confidence intervals (CIs), and diamonds pooled HRs and 95% CIs. AgeDev, age deviation.

Fig. 3

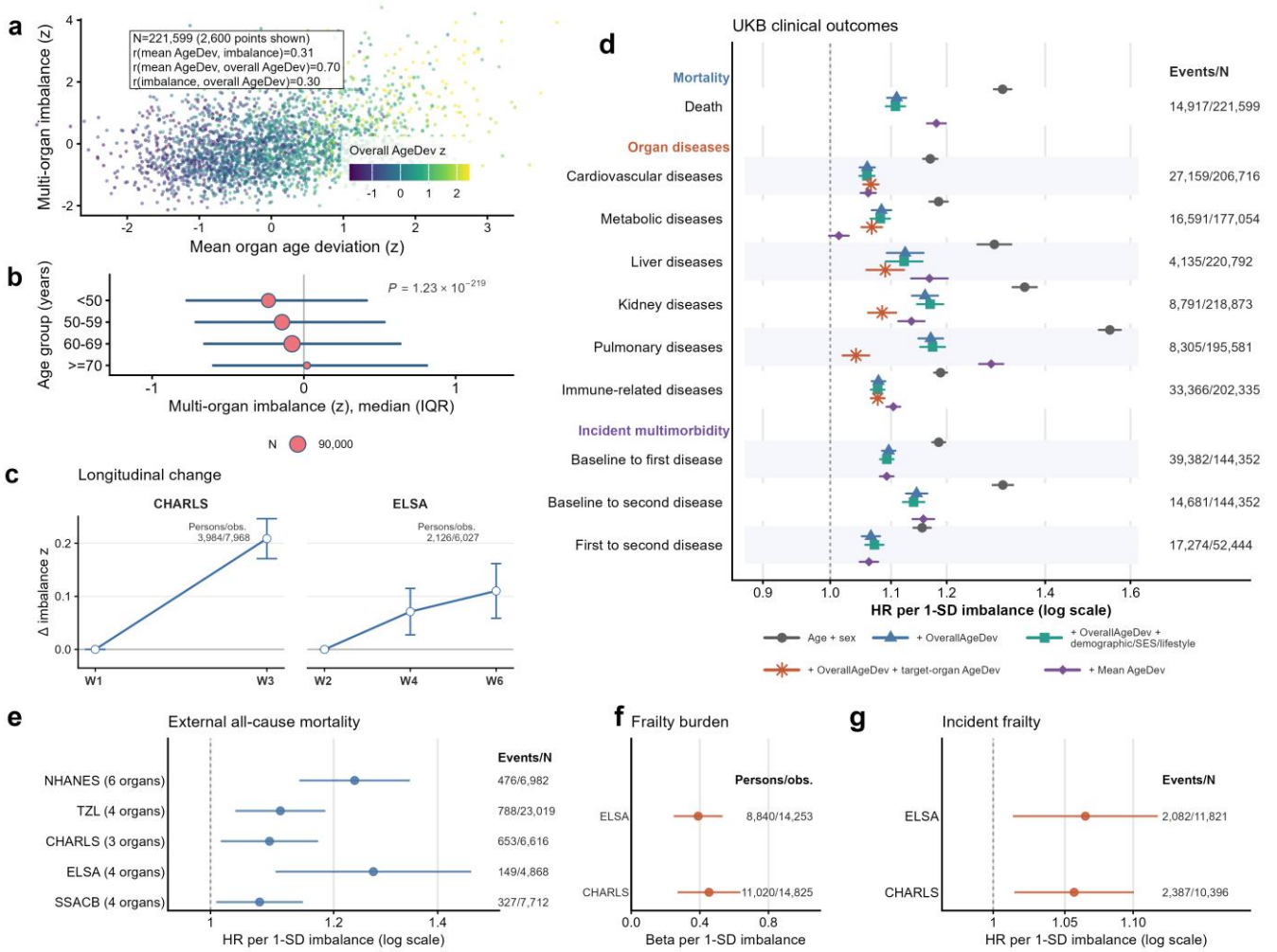


Fig. 3 | Multi-organ imbalance is associated with multiple adverse health outcomes across cohorts. a, Relation of multi-organ imbalance to mean organ AgeDev in 221,599 UKB participants; colour represents overall AgeDev. For display, 2,600 participants are shown; Pearson correlations use all 221,599 participants. **b,** Multi-organ imbalance across chronological-age groups in UKB. Points denote medians, horizontal bars interquartile ranges (IQRs), and point size the number of participants. The displayed two-sided *P* value is from a Kruskal–Wallis test. **c,** Mean within-person change in imbalance from the reference wave to subsequent waves in CHARLS and ELSA. Error bars denote *t*-based 95% CIs; numbers give participants and person-wave observations. **d,** Associations of imbalance with all-cause mortality, six incident organ-disease outcomes and three multimorbidity transitions in UKB. Estimates are shown for models adjusted for chronological age and sex; the primary model additionally adjusted for overall AgeDev; two branches added demographic, technical, socioeconomic and lifestyle covariates or the outcome-matched organ AgeDev; and a parallel model used mean organ AgeDev in place of overall AgeDev. The outcome-matched adjustment applies only to organ-disease outcomes. **e,** Associations with all-cause mortality in five external cohorts, adjusted for mean organ AgeDev, chronological age and sex. The number of organs contributing to each cohort-specific imbalance measure is given in parentheses. **f,** Association with repeated frailty-index burden in ELSA and CHARLS, estimated using generalized estimating equations adjusted for mean organ AgeDev, chronological age and sex. Coefficients represent frailty-index percentage-point differences per 1-s.d. higher imbalance. **g,** Associations with incident frailty in repeated-landmark Cox models adjusted for the same covariates. Counts indicate event records/landmark records. In **d**, **e** and **g**, points denote HRs and horizontal bars 95% CIs; in **f**, they denote regression coefficients and 95% CIs. AgeDev, age deviation; HR, hazard ratio; IQR, interquartile range; SES, socioeconomic status.

Fig. 4

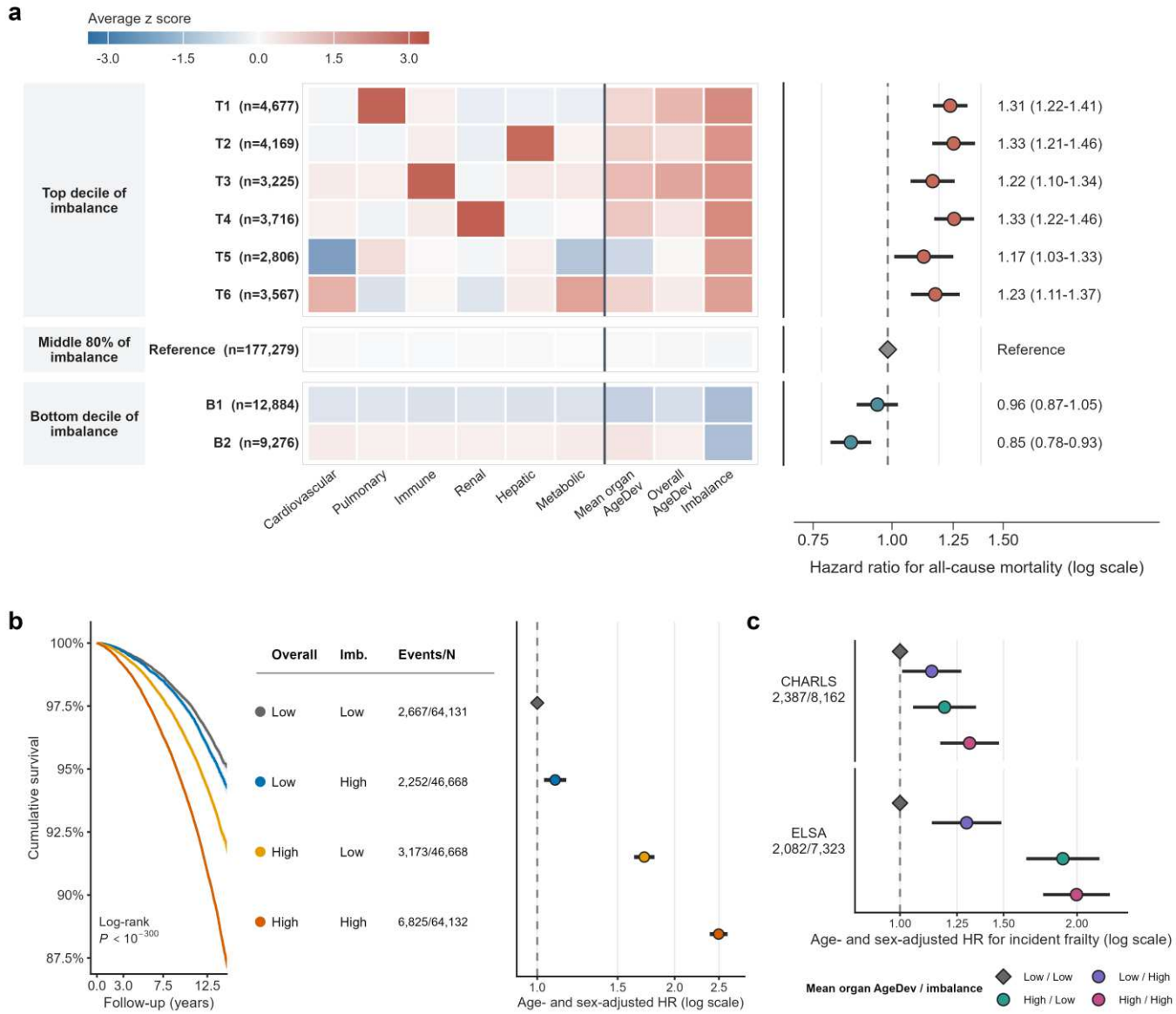


Fig. 4 | Multi-organ imbalance stratifies risk within levels of overall aging. a, Mean organ-aging profiles and associated mortality estimates among participants in the top and bottom deciles of the UKB imbalance distribution. K-means clustering of the six organ AgeDev *z*-scores was used to derive six top-decile profiles (T1–T6). Because the bottom-decile profiles were largely concordant and data-driven diagnostics favoured a single cluster, two descriptive profiles (B1–B2) were fixed to examine variation within the low-imbalance tail. The middle 80% formed the reference group. Cell colour denotes the profile mean of each standardized measure, and row labels give profile sizes. The adjacent forest plot shows associations of the eight tail profiles with all-cause mortality relative to the middle 80%, adjusted for overall AgeDev, chronological age and sex. Points denote hazard ratios (HRs) and horizontal bars 95% confidence intervals (CIs). **b,** All-cause mortality across joint strata defined by median overall AgeDev and median imbalance. The left panel shows Kaplan–Meier survival curves; the displayed two-sided *P* value is from a log-rank test. The right panel shows age- and sex-adjusted HRs and 95% CIs relative to Low/Low. Events and risk-set sizes are displayed for each stratum. **c,** Incident frailty across corresponding mean organ AgeDev and imbalance strata in CHARLS and ELSA. Models used Low/Low as the reference and were adjusted for chronological age and sex. Counts indicate event records/unique participants; participants could contribute more than one landmark record. AgeDev, age deviation.

Fig. 5

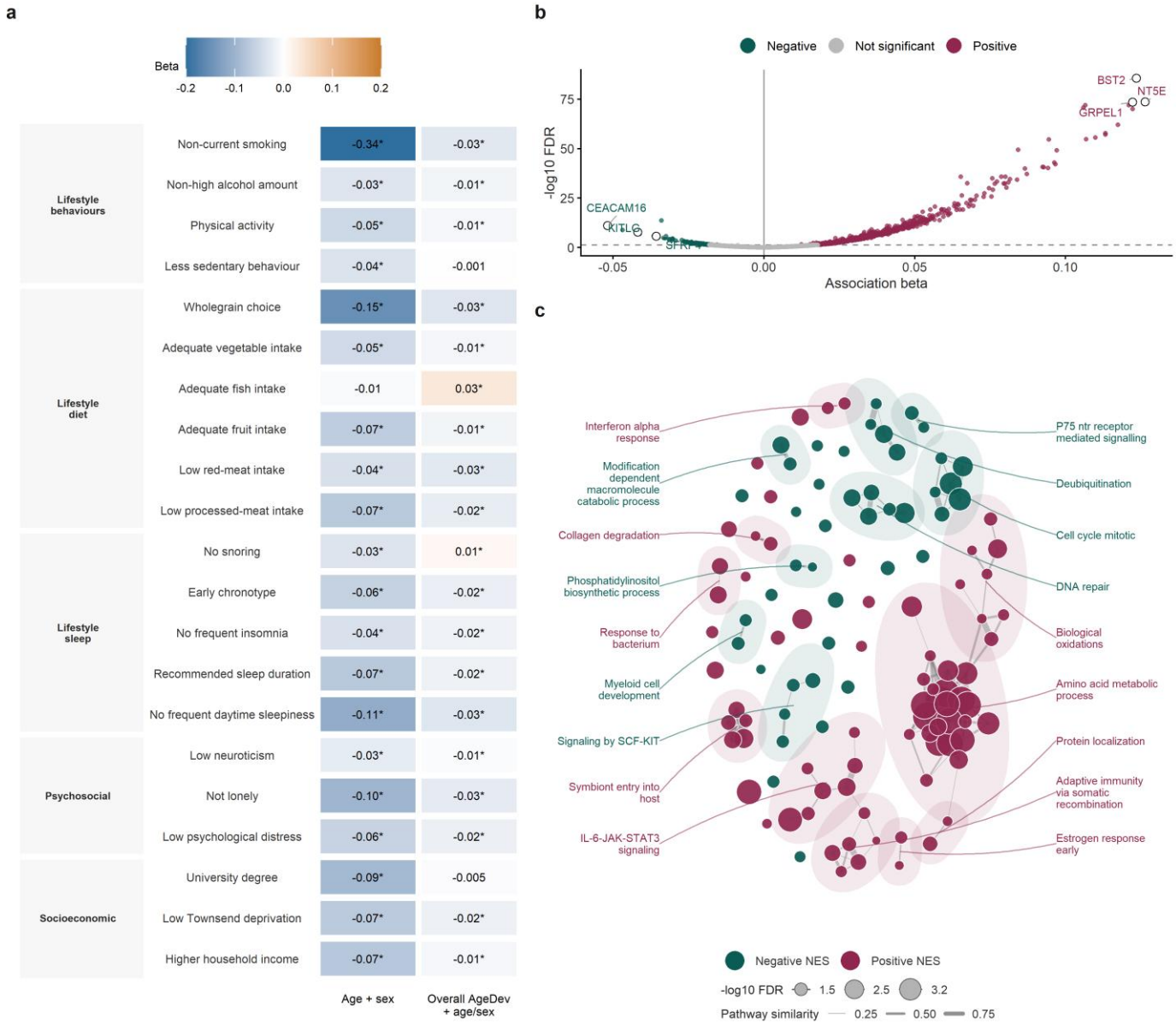


Fig. 5 | Exposure and proteomic correlates of multi-organ imbalance. a, Associations of 21 favourably coded behavioural, dietary, sleep, psychosocial and socioeconomic indicators with phenotype-derived imbalance in UKB. Separate linear models adjusted for chronological age and sex and then additionally for overall AgeDev. Continuous indicators were standardized and binary indicators were analysed as 1 versus 0. Cell colour and text give the regression coefficient; asterisks denote Benjamini–Hochberg false-discovery rate (FDR) < 0.05 within the displayed model. **b,** Associations of 2,916 standardized plasma proteins with phenotype-derived imbalance in 19,744 UKB participants, adjusted for overall AgeDev, chronological age, sex and body mass index. The x axis gives the difference in standardized protein abundance per 1-s.d. higher imbalance and the y axis gives −log10 FDR. Colours distinguish positive, negative and non-significant associations at FDR < 0.05. **c,** Network summary of FDR-significant pathways identified by gene-set enrichment analysis of the ranked protein associations. Node colour denotes the direction of the normalized enrichment score (NES), node size −log10 FDR, and edge width pathway similarity; shaded regions group related pathways into descriptive modules. Multi-pathway modules are labelled by the pathway with the lowest database-family-specific FDR. AgeDev, age deviation; FDR, false-discovery rate; NES, normalized enrichment score; SES, socioeconomic status.

Fig. 6

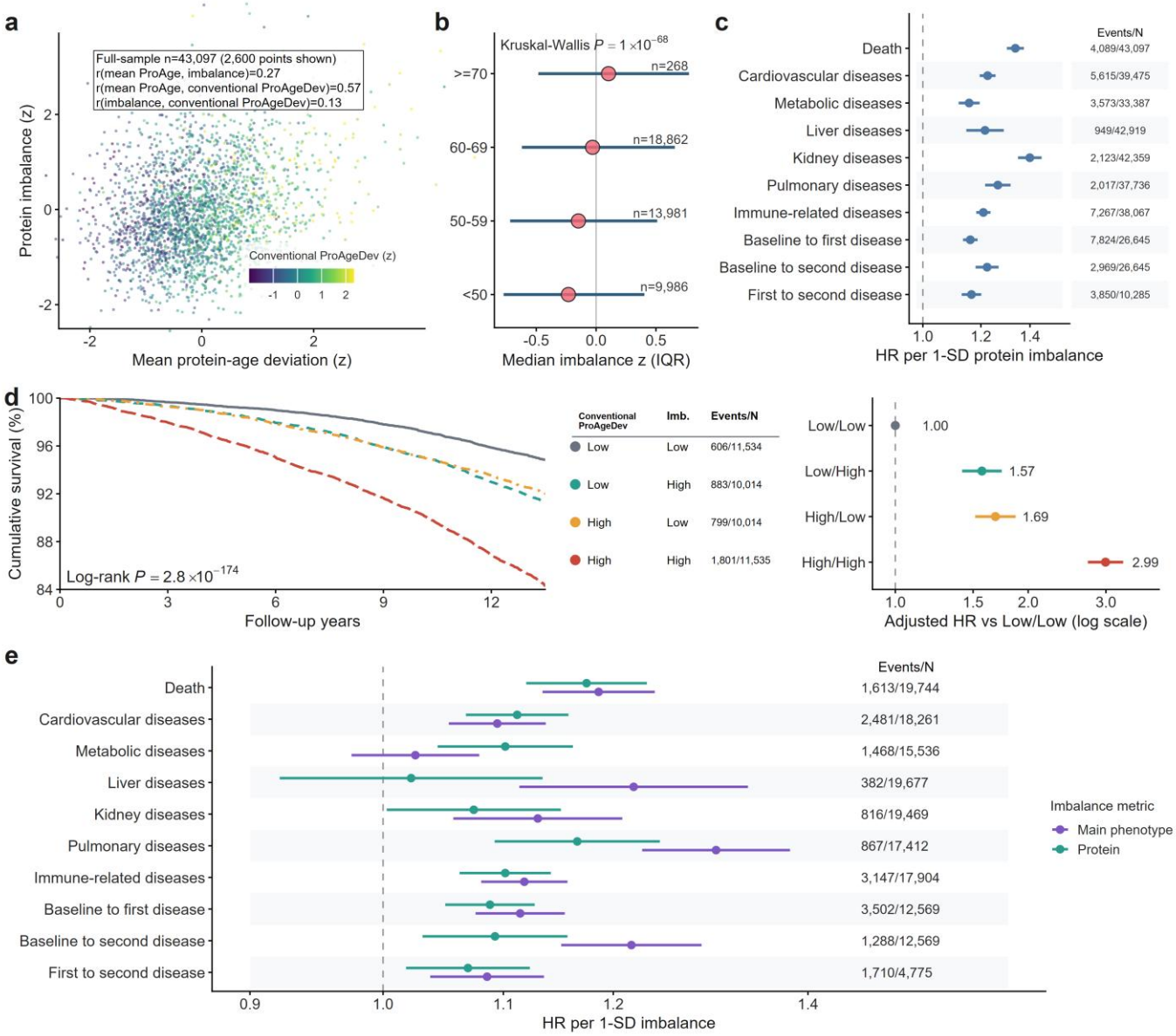
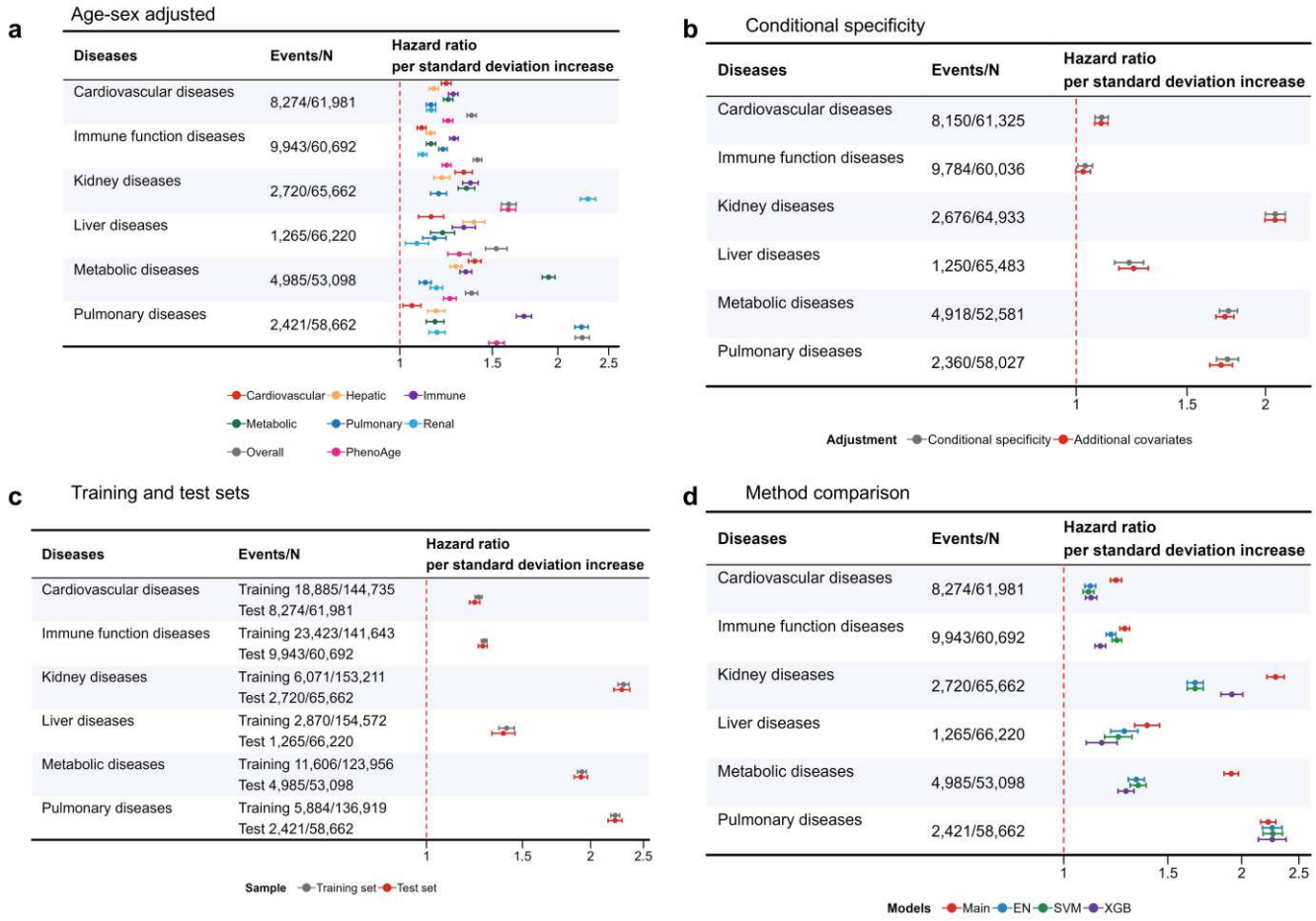


Fig. 6 | Multi-organ imbalance extends to protein-derived organ aging. a, Relationships among protein-derived imbalance, mean organ ProAge deviation and conventional ProAge deviation in 43,097 UKB participants. Imbalance is plotted against mean organ ProAge deviation, with colour representing conventional ProAge deviation; for display, 2,600 participants are shown; Pearson correlations use all 43,097 participants. **b,** Protein-derived imbalance across chronological-age groups. Points denote medians, horizontal bars interquartile ranges (IQRs), and labels group sizes. The displayed two-sided *P* value is from a Kruskal–Wallis test. **c,** Associations of protein-derived imbalance with all-cause mortality, six incident organ-disease outcomes and three multimorbidity transitions, adjusted for conventional ProAge deviation, chronological age and sex. Estimates are reported per 1-s.d. higher protein-derived imbalance. **d,** All-cause mortality across joint strata defined by median conventional ProAge deviation and median protein-derived imbalance. Kaplan–Meier curves are shown on the left; the displayed two-sided *P* value is from a log-rank test. Age- and sex-adjusted hazard ratios (HRs) relative to Low/Low are shown on the right. **e,** Common-sample comparison of phenotype-derived and protein-derived imbalance associations in 19,744 participants. For each outcome, the two measures were fitted on identical participant rows; phenotype-derived models adjusted for mean organ AgeDev, chronological age and sex, and protein-derived models adjusted for mean organ ProAge deviation, chronological age and sex. Points denote HRs and horizontal bars 95% confidence intervals (CIs). AgeDev, age deviation; ProAge, protein-derived age.

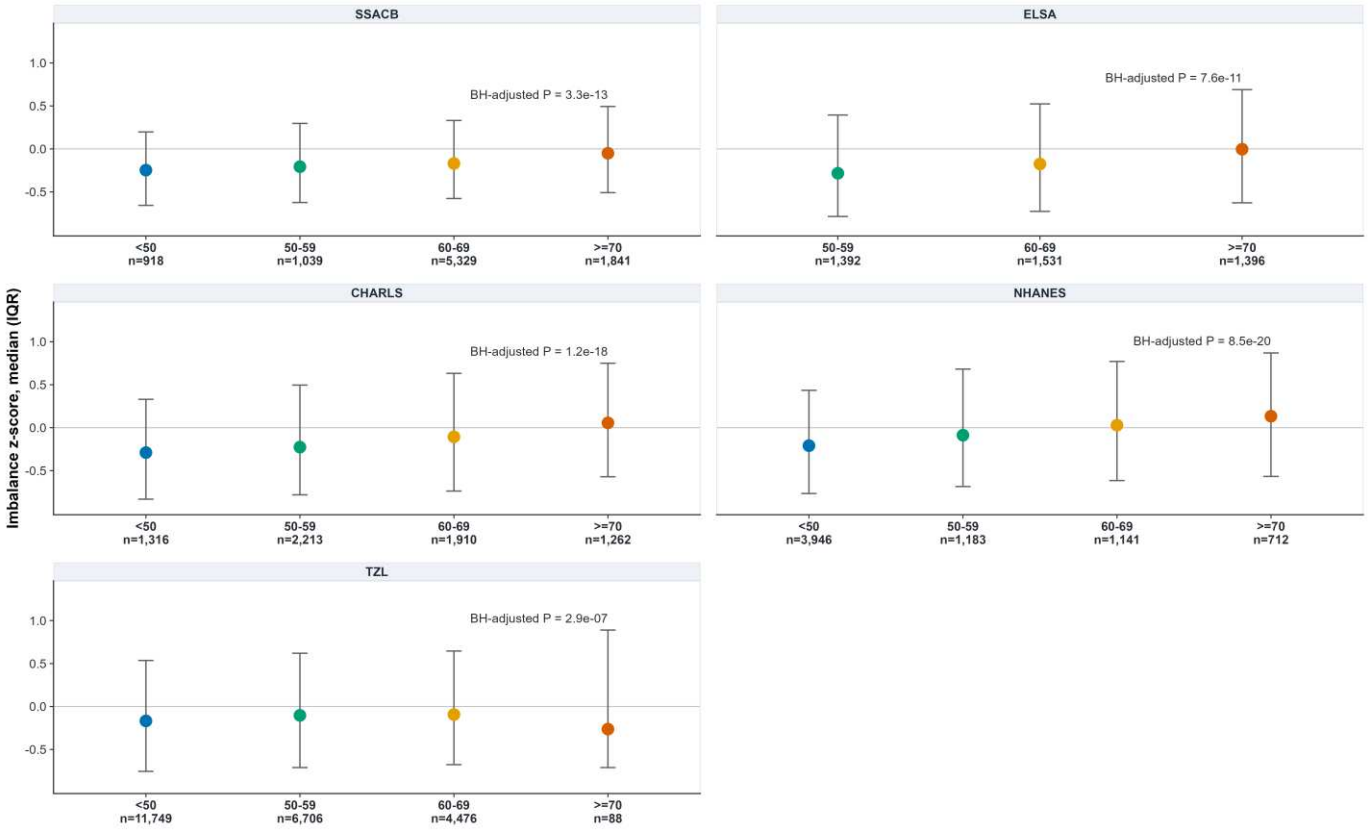
Extended Data figures

Extended Data Fig. 1



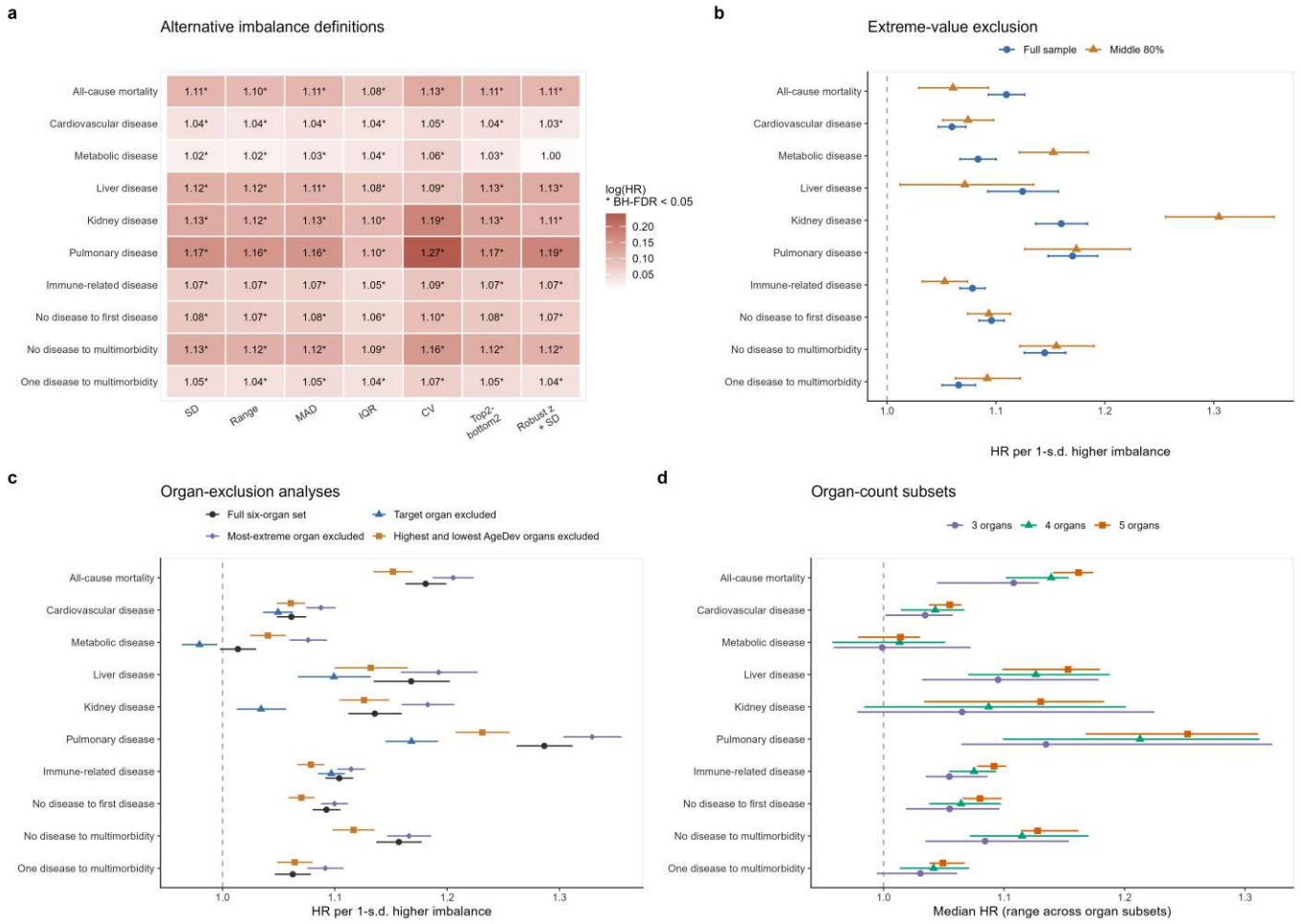
Extended Data Fig. 1 | Internal evaluation of phenotype-derived organ biological ages. a, Separate associations of the six organ AgeDev measures, overall AgeDev and PhenoAge deviation with each incident organ-disease outcome in the UKB test set, adjusted for chronological age and sex. **b,** Outcome-matched organ AgeDev estimates from mutually adjusted conditional-specificity models before and after additional adjustment for ethnicity, smoking, alcohol consumption and education; the two models used identical complete-case samples. **c,** Outcome-matched estimates from separate age- and sex-adjusted models in the UKB training and test sets. **d,** Descriptive comparison of matched organ-disease estimates from the primary organ-age models and biological ages derived using elastic-net regression, linear support vector machine regression (SVM) and XGBoost in common test-set samples. All estimates are reported per 1-s.d. higher AgeDev. Points denote hazard ratios and horizontal bars 95% confidence intervals. AgeDev, age deviation; EN, elastic-net regression; SVM, support vector machine regression; XGB, XGBoost.

Extended Data Fig. 2



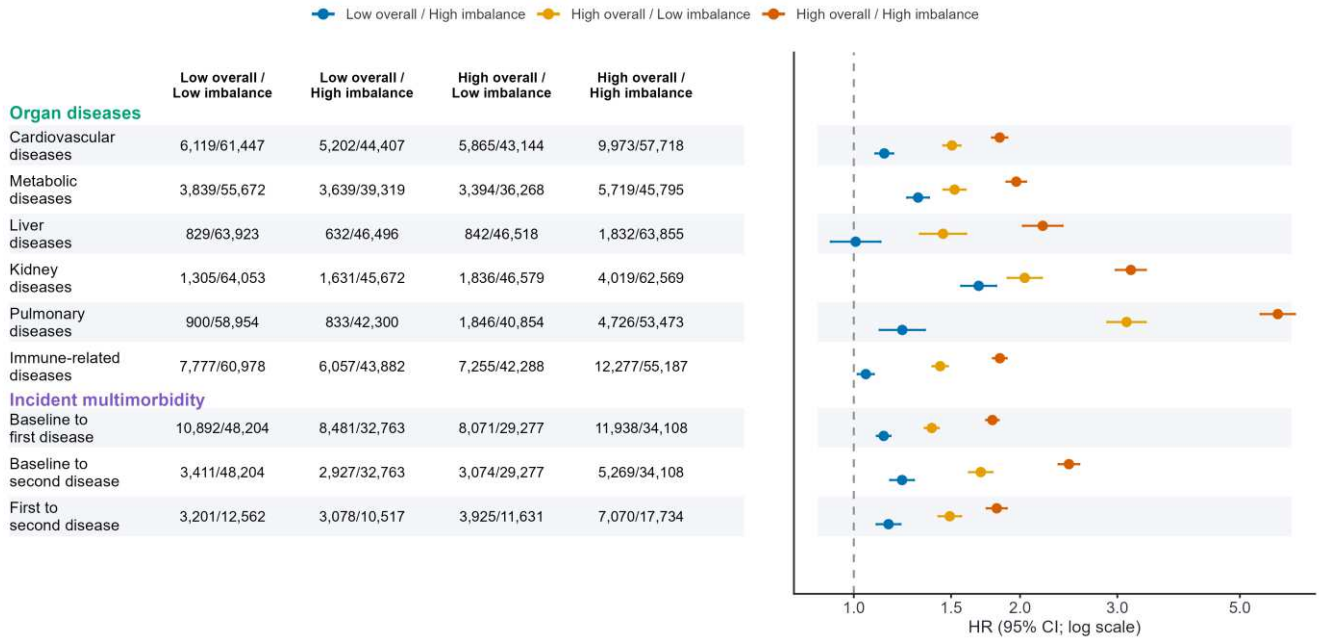
Extended Data Fig. 2 | Multi-organ imbalance across chronological-age groups in external cohorts. Cohort-specific distributions of phenotype-derived imbalance in SSACB, ELSA, CHARLS, NHANES and TZL. Points denote medians, vertical bars interquartile ranges, and labels group sizes. Imbalance was calculated from the organ systems available in each cohort and retained the scale defined in the corresponding fixed reference sample. Displayed two-sided *P* values are from Kruskal–Wallis tests and were adjusted across cohorts using the Benjamini–Hochberg procedure.

Extended Data Fig. 3



Extended Data Fig. 3 | Sensitivity analyses of phenotype-derived multi-organ imbalance in UK Biobank. a, Hazard ratios (HRs) for mortality, incident organ disease and multimorbidity transitions using the primary within-person standard deviation, range, mean absolute deviation (MAD), interquartile range (IQR), coefficient of variation (CV), top-two versus bottom-two mean difference, and imbalance after median/MAD organ standardization. Cell text gives the HR per 1-s.d. higher metric and colour represents log(HR); asterisks denote Benjamini–Hochberg false-discovery rate <0.05 across all 70 metric–outcome tests. **b,** Primary associations in the full sample and after restriction to the middle 80% of the imbalance distribution. **c,** Associations after excluding the outcome-matched organ, the participant-specific most-extreme organ, or both the highest and lowest organ values. **d,** Median HRs and ranges across all three-, four- and five-organ subsets. Mean organ AgeDev and imbalance were reconstructed together for each altered organ set or standardization. All models included chronological age and sex, with additional adjustment for mean organ AgeDev and overall AgeDev in a, overall AgeDev in b, and the corresponding reconstructed mean organ AgeDev in c and d. Outcome-matched organ exclusion was not applicable to mortality or multimorbidity. In **b–d**, points denote HRs or median HRs and horizontal bars 95% confidence intervals or ranges across subsets, as labelled. AgeDev, age deviation.

Extended Data Fig. 4



	Low overall / Low imbalance	Low overall / High imbalance	High overall / Low imbalance	High overall / High imbalance
Organ diseases				
Cardiovascular diseases	6,119/61,447	5,202/44,407	5,865/43,144	9,973/57,718
Metabolic diseases	3,839/55,672	3,639/39,319	3,394/36,268	5,719/45,795
Liver diseases	829/63,923	632/46,496	842/46,518	1,832/63,855
Kidney diseases	1,305/64,053	1,631/45,672	1,836/46,579	4,019/62,569
Pulmonary diseases	900/58,954	833/42,300	1,846/40,854	4,726/53,473
Immune-related diseases	7,777/60,978	6,057/43,882	7,255/42,288	12,277/55,187
Incident multimorbidity				
Baseline to first disease	10,892/48,204	8,481/32,763	8,071/29,277	11,938/34,108
Baseline to second disease	3,411/48,204	2,927/32,763	3,074/29,277	5,269/34,108
First to second disease	3,201/12,562	3,078/10,517	3,925/11,631	7,070/17,734

Extended Data Fig. 4 | Joint overall AgeDev and imbalance strata across UK Biobank disease and multimorbidity outcomes. Events and risk-set sizes are shown for Low/Low, Low/High, High/Low and High/High strata defined by the population medians of overall AgeDev and imbalance. Forest plots show age- and sex-adjusted hazard ratios and 95% confidence intervals for the three non-reference strata relative to Low/Low across six incident organ-disease outcomes and three multimorbidity transitions. AgeDev, age deviation.